北海道大学
HOKKAIDO UNIVERSITY

Doctoral Dissertation

Transport Model Diagnosis of Stratospheric Transport Field Using Boundary Impulse Evolving Response Method

Nguyen Thi Hanh

Division of Earth System Science
Graduate School of Environmental Science
Hokkaido University

August, 2021

Acknowledgements

In the past, I had never thought that I would come to Japan for my studying. However in a twist of fate, my supervisor *Prof. Fumio Hasebe* who had visited Vietnam National University, VNU_University of Science, university paved my way to Hokkaido University of Japan for my PhD study in a totally brand new yet fascinating topic for me. The journey in completing my PhD and hence this thesis is full of overwhelming challenges, and I would not be able to make it this far without the tireless efforts and guidance from my supervisor. He has spent tremendous time and energy in making sure that I could understand my topic of study, and correcting a lot of my silly mistakes. I am also very grateful to him for allowing me to use his work on Lagrangian method in this thesis, for comparison with my work, enhancing the content of this thesis. Without him, this work would not have been realized. At the same time, I also owe *Assoc. Prof. Masatomo Fujiwara* a great debt for taking me under his wings when Prof. Hasebe retired, and giving me a lot of encouragements and valuable advices.

I would like to express my great gratitude to *Dr. Kentaro Ishijima* from Japan Agency for Marine-Earth Science and Technology (JAMSTEC) for providing and allowing me to use his ACTM data in this thesis as well as his encouragement and constructive comments. Special thanks are given to *Dr. Satoshi Sugawara* from Miyagi University of Education for his assistance on testing the sensitiveness of a parameter from CUBE/Biak

observed air samples and his valuable comments.

I would like show my appreciation to *Prof. Yoichi Tanimoto*, *Prof. Takeshi Horinouchi* (Graduate School of Environmental Science), *Dr. Hideharu Akiyoshi* (National Institute for Environmental Studies, NIES) and *Assoc. Prof. Masatomo Fujiwara* who are members of the dissertation committee of the Graduate School of Environmental Science for their valuable reviews for this study to be improved. I also want to thank organizations that funded for my study, including the Special Grant Program for International Students of *Graduate School of Environmental Science of Hokkaido University*, Japan Student Services Organization (*JASSO*), and Foreign Student Scholarship of Hokkaido International Exchange & Cooperation Center (*HIECC*).

I acknowledge the help of *Dr. Dmitry Belikov* for providing me the NIES transport model data and helping me on understanding about a chemical transport model. The data has also been very useful to me in learning the necessary calculations which I later applied in this study. Not forgetting are the *members in Prof. Hasebe's and Assoc. Prof. Fujiwara's lab*, who have lend me support and providing me with various constructive comments to my work. A heart felt thank you to *Ms. Kakuno* and the *staffs in the Atmosphere-Ocean and Climate Dynamics Course* for helping me with my Japanese documents. Also, I am grateful to my *officemates* for creating a delightful atmosphere throughout my working years here.

I want to extend my deepest thanks to my *grandmother and both parents* for their love and supports. Special thanks to my *friends* for always listening to and encouraging me. And most importantly, a person whom I am unable to express my thanks in words is my *life partner*, Dr. Chung Jing Xiang. He always believes in me even when I have doubted myself. He motivates me each time I want to give up. Without him, I could not complete this voyage.

Abstract

Transport model diagnosis of stratospheric transport field using boundary impulse response method

Atmospheric transport plays an important role on the distribution of stratospheric trace gases. Changes in their concentrations potentially have a strong impact on global climate. Since the tropospheric air mostly enters the stratosphere through the tropical tropopause layer (TTL), the age of air, the transit time since stratospheric air parcel last had contact with the troposphere, is used as a common proxy of the transport. The mean age of air provides understanding in the strength of stratospheric circulation. Because of the irreversible mixing, any air parcel is composed of many elements that have taken different pathways. Thus, mean age can not be characterized by a single transit time, but by a distribution of transit times. This distribution is the age spectrum, which provides the full information about transport histories of parcels. It is not directly observable, but can be obtained by applying the boundary impulse evolving response (BIER) method that uses simulated distribution of inert tracers released as a series of pulses at a source region.

This study applies the BIER method with the aid of an atmospheric general circulation model-based chemistry transport model (ACTM) nudged to ERA-Interim meteorological fields to investigate stratospheric transport field. Multi-year averaged transport field is examined by comparing the evolution and distribution of tracers with the source region at tropical surface and at the TTL. The results show a rapid transport toward high-latitude lowermost stratosphere due to the eddy mixing around the tropopause. Stratospheric transport features are also shown through the variations of age spectrum. Multi-peaks of age spectrum reflect the seasonal variations of the stratospheric circulation and isentropic mixing. The results are also applied to assess the

mean age estimated from CO_2 and SF_6 samples acquired during a field campaign over Indonesia. Comparisons are also made with those estimated from Lagrangian backward trajectories calculated by using the ACTM transport field. The mean age derived from the BIER method is noticeably older than that estimated by the Lagrangian method and the stratospheric air samples, implying high diffusivity in the transport model. In contrast, observed SF_6 age is only reproducible in lower stratosphere, and far exceeds the estimates from the Lagrangian method above 25 km.

This study confirms the capability of BIER method in capturing all transport features including unresolved diffusive processes. Mean age estimation by this method with the source region at the TTL does not work well due to its wide coverage in latitude and height. The study also highlight the difficulty in estimating mean age from air samples assuming a ratio between the first and the second moments of the age spectrum. The transport field simulated by the ACTM indicates height dependency of this ratio in the tropical lower stratosphere.

Table of Contents

List of publications

Nguyen, T. H., K. Ishijima, S. Sugawara, and F. Hasebe, (2021): Application of a nudge general circulation model to the interpretation of the mean age of air derived from stratospheric samples in the tropics, J. Meteor. Soc. Japan, 99, doi:10.2151/jmsj.2021-056, 2021.

List of Abbreviations

ACTM	Atmospheric general circulation model-based Chemistry Transport Model
AoA	age of air
BDC	Brewer-Dobson circulation
BIER	boundary impulse evolving response
BIR	boundary impulse response
CLaMS	Chemical Lagrangian Model of the Stratosphere
CONTRAIL	Comprehensive Observation Network for TRace gases by AIrLiner
CUBE/Biak	Coordinated Upper-Troposphere-to- Stratosphere Balloon Experiment in Biak
ERA-Interim	European Centre for Medium-Range Weather Forecasts Interim
GCM	general circulation model
LCP	Lagrangian cold point
LS	lower stratosphere
NH	Northern hemisphere
PDF	probability distribution function
QBO	Quasi-Biennial Oscillation
SH	Southern hemisphere
TEM	Transformed Eulerian Mean
$\mathrm{Tr}_{\mathrm{top}}$	top of the tropical troposphere
TST	Troposphere-to-stratosphere transport

TTL	tropical tropopause layer
UGAMP	United Kingdom Universities' Global Atmospheric Modelling Programme
UTLS	Upper troposphere lower stratosphere
WMO	World Meteorological Organization

Chapter 1

Introduction

1.1 Motivation of study

Stratospheric transport plays an important role on distributions as well as chemical lifetimes of many trace gases (tracers), such as water vapor (H_2O), ozone (O_3), chlorofluorocarbons (CFCs), carbon dioxide (CO_2), sulfur hexafluoride (SF_6) and methane (CH_4) in the stratosphere. This is because changes in concentrations of tracers potentially have a strong impact on radiation balance of the Earth's surface and life on Earth as well. For example, although water vapor has a very low concentration in the stratosphere, the infrared emission through it and the convection-induced vertical flux of heat has significant impact on the temperature of troposphere and stratosphere. It is also demonstrated that an observed quick decline of stratospheric water vapor around 2000–2001 (Randel et al., 2006; Scherer et al., 2008; Fujiwara et al., 2010) could have affected the rate of increase of global surface temperature (Solomon et al., 2010; Riese et al., 2012). Although ozone, the shield to protect life on Earth, is mainly formed in the tropical stratosphere,

its high concentration is found in high latitudes. It has been destroyed by anthropogenic released long-lived CFCs (World Meteorological Organization, 1995). Long-lived tracers

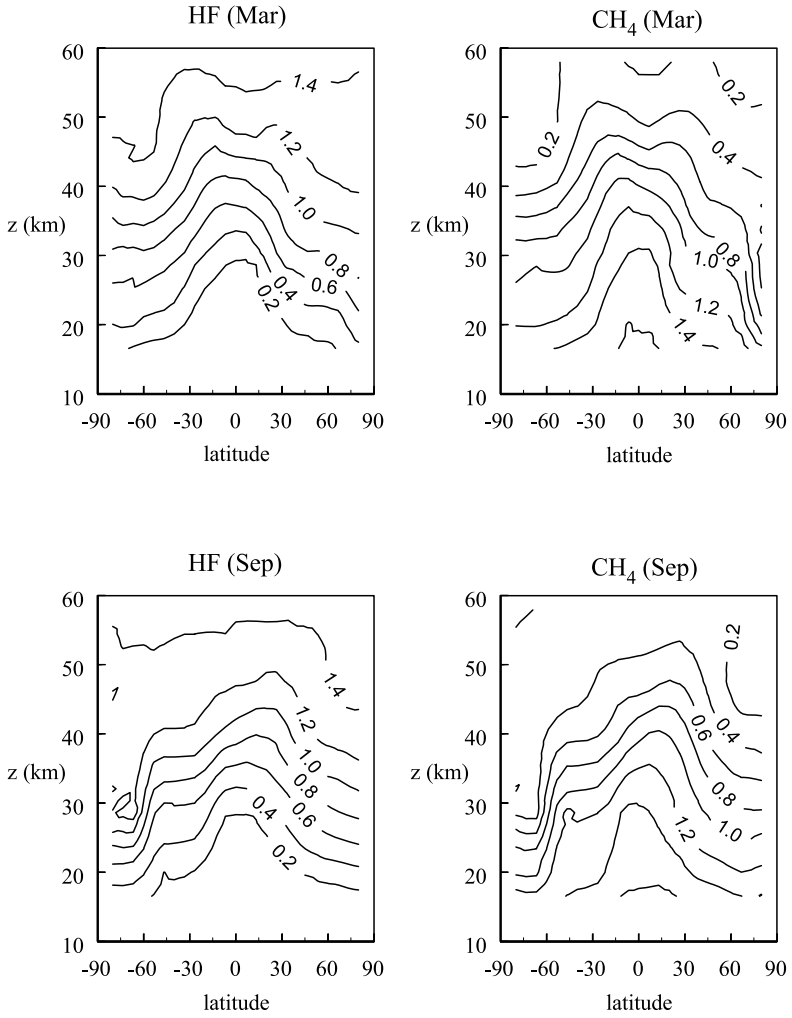

Figure 1.1: Meridional distribution of HF and CH_4 from the Halogen Occultation Experiment instrument from Plumb (2007). ©American Geophysical Union. Used with permission.

such as hydrogen fluoride (HF) and CH4 are found to have quite similar distribution of isopleths at the same time. Figure 1.1 shows the zonal mean distribution structure of HF and CH_4 in the stratosphere in March and September attained from the Halogen Occultation Experiment instrument. HF has its source and sink in the stratosphere and

troposphere, respectively. Meanwhile, CH_4 has its source in the troposphere and its sink in both troposphere and stratosphere. The structure of mixing ratio isopleths between two tracers is quite similar in the same month, including an upward bulge in the tropics and poleward slopes in the extratropics. The mixing ratio isopleths tend to be flattened in midlatitudes. Large horizontal gradients of mixing ratio take place at the edges of subtropical jet and polar vortex in mid-latitude winter hemisphere. Such distribution is also found in nitrous oxide (N_2O) distribution (Jones and Pyle, 1984). Moreover, seasonal variation in the distribution of these tracers is suggesting seasonal change in the stratospheric transport (Chen, 1995; Rosenlof et al., 1997; Ray et al., 1999). These imply an important role of stratospheric transport processes to the stratospheric distribution of species. Therefore, tracers, especially long-lived tracers, are very important for investigating the transport features. Unfortunately, observations of stratospheric tracers are limited. Hence, modeling is requested to improve understanding and insights on characteristics of the stratospheric transport field as well as the distribution and variability of principal tracers.

Stratospheric transport is mainly dominated by a stratospheric circulation, named Brewer-Dobson circulation (BDC), and a quasi-horizontal transport and mixing, as seen in Fig. 1.2. As stratospheric transport information is fully contained in stratospheric long-lived tracers' distribution, and as those tracers partly have tropospheric origin, the age of air (AoA), the transit time that an air parcel takes for transport to occur from the troposphere to different regions in the stratosphere, is introduced as a useful representative of for analysis of transport (Kida, 1983; Hall and Plumb, 1994). The younger the AoA is, the stronger the stratospheric circulation and mixing are. Modulation of the BDC, such as changes in its velocities, mass transport and pathways, can thus be quantified by the AoA. The AoA can be directly computed through a "clock tracer", whose concentration of inert tracer linearly increases with time, by considering

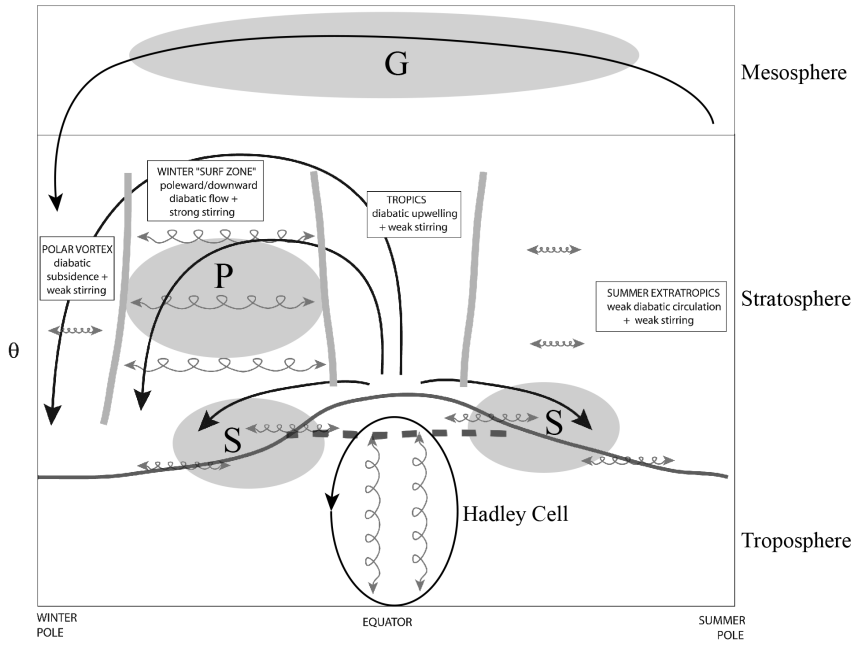

Figure 1.2: Schematic diagram of atmospheric transport, modified from Plumb (2002, 2007). Thick solid line from North to South pole represents the tropopause. Dashed line shows the bottom of the tropical tropopause layer. Gray vertical lines are the transport barriers at the edges of subtropical eddy and polar vortex. Curled two-head arrows denote the horizontal mixings. P, S, and G denote regions of breaking planetary scale waves, synoptic scale waves and gravity waves, respectively. ©American Geophysical Union. Used with permission.

the time lag of its concentration growth between the tropospheric source and the stratosphere (Schmidt and Khedim, 1991) as illustrated in Fig 1.3. The source region in the troposphere is regarded as "reference". Nevertheless, no measured trace gas is real clock tracer. Tracers such as CO_2 and SF_6, given their anthropogenically driven nearly linear increase and chemically conservative nature make it possible to use their stratospheric mixing ratio as a lag time of their entry into the stratosphere, are commonly used in lieu. As such, the lag time of the time-series of CO_2 and SF_6 in the stratosphere relative to the time-series in the troposphere can be used as a measure of the mean age (Elkins et al., 1996; Boering et al., 1996; Harnisch et al., 1996; Patra et al., 1997; Andrews et al., 2001b). In general, the age estimated from observations of different tracers is comparable, aside

from overestimated SF_6 age in the polar vortex in which it is affected by mesospheric SF_6 loss (related to the descent of mesospheric circulation in Fig. 1.2) (Waugh and Hall, 2002). However, any air parcel is composed of many elements, each with a different

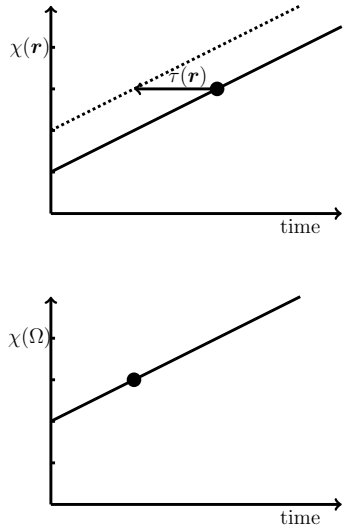

Figure 1.3: Schematic diagram of the time series of a clock tracer at a stratospheric location of interest $\boldsymbol{r}$. Time series at the source region (troposphere) $\boldsymbol{\Omega}$ is shown in dotted line. $\tau(\boldsymbol{r})$ is the time lag between a particular tracer mixing ratio at $\boldsymbol{r}$ and its mixing ratio at $\boldsymbol{\Omega}$. Adapted from Waugh and Hall (2002). ©American Geophysical Union. Used with permission.

transport pathway and transit time (Kida, 1983). Such multiple pathways taken by the elements pose a fundamental difficulty in interpreting the AoA. A complete description of the age of a given air parcel is thus captured by the age spectrum, which is a statistical distribution of the element transit times (Kida, 1983; Hall and Plumb, 1994; Waugh and Hall, 2002). The age spectrum provides the full information about transport histories of air parcels, including mean age (first moment), modal age (peak of age spectrum) and spectrum width (second moment).

Due to variations of the stratospheric transport, the stratospheric age spectrum shape varies at different locations. Figure 1.4 illustrates schematically shapes of age spectrum in the tropical lower stratosphere (right) and the rest of stratosphere (left).

In the tropics wherein the upwelling occurs, the age spectrum shows a strong peak at a very short transit time and a short tail. On the other hand, in the extratropics and

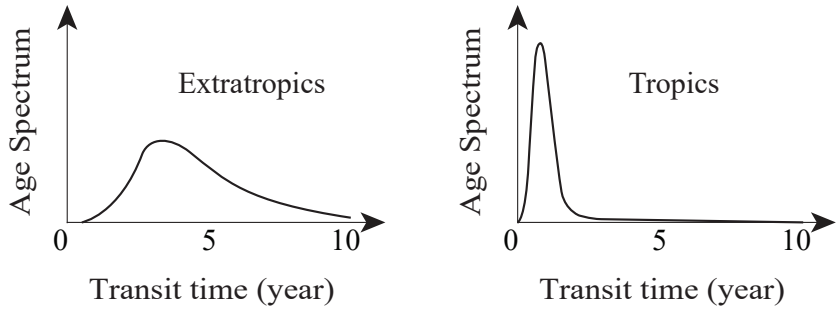

Figure 1.4: Schematic diagram of typical age spectrum in the tropical lower stratosphere (right) and extratropics (left). Adapted from Waugh and Hall (2002). ©American Geophysical Union. Used with permission.

high altitudes, the age spectrum is broad with a long tail and peak at longer transit time due to multiple pathways with various transit times caused by the slow circulation and mixing. The slower is the decrease of the age spectrum tail, the larger is the first moment. Therefore, the mean age is young in tropics and gradually becomes older in extratropics and high altitudes. Waugh and Hall (2002) showed that the mean age is about 1 year in the tropics and increases to ~ 4 years in high latitudes of lower stratosphere. Unlike distribution of many tracers which have tropospheric origin, the mean age increases with altitude, reaching values of $\sim 4-5$ years at 30 km in the tropics and 6 years at high latitudes.

The age spectrum cannot be directly observed like as the AoA. It can be indirectly estimated from measurements of tracers, whose concentration linearly increases with time in the troposphere, by assuming a stationary flow and a spectrum shape (Hall and Plumb, 1994) via a ratio of moments between the first and second moments of age spectrum. However, this method most probably underestimates the spectrum tail (Hauck et al., 2019). Uncertainties related to this assumption still need further discus-

sions. Furthermore, the age spectrum can be estimated from models. Hall and Plumb (1994) estimated the age spectrum as the time development of an artificial inert tracer in a pulse release experiment in a general circulation model (GCM). This method is direct and straightforward. But an assumption of stationary flow is the limitation. This is because in real atmosphere flow is unsteady. Therefore, this method is unusable to study the seasonality of the age spectrum. Holzer et al. (2003) and Haine et al. (2008) addressed this limitation of Hall and Plumb (1994)'s method by implementing an ensemble of pulse release experiments. The direct output of this method, time-series of tracer mixing ratio, is the boundary impulse response (BIR), but not the age spectrum. The age spectrum is obtained through a number of BIRs. This improved method is known as the BIR method (Li et al., 2012a,b) or the boundary impulse evolving response (BIER) method (Ploeger and Birner, 2016). Moreover, Lagrangian trajectory calculation, by tracing a large number of air parcels in a three-dimensional wind field by backward trajectories (Schoeberl et al., 2003; Fueglistaler et al., 2005; Hasebe et al., 2018), is also one of choices for the age spectrum computation although it demands computational resources and ignores unresolved mixing. Different methods, even shortcomings in each method, can result in discrepancies in the estimation of mean age. Additionally, uncertainties on measurements such as seasonal variation of tropospheric CO_2 or loss of SF_6 from mesosphere to stratosphere, also contribute to the mean age difference.

Estimation of the long-term trend of mean age after careful consideration of the non-linearity in the growth of accumulated observations of CO_2 and SF_6 mole fractions in the northern midlatitude stratosphere (e.g., Schmidt et al., 1987; Nakazawa et al., 1995; Engel et al., 2002) showed an increase (though not statistically significant) at a rate of 0.15 ± 0.18 years decade^{-1} (Engel et al., 2017). Although this rate has been reduced to 0.07 ± 0.16 years decade^{-1} by a recent study (Fritsch et al., 2020), these estimates are still apart from the long-term decrease of mean age diagnosed by chemistry–climate

models (Austin et al., 2007; Waugh, 2009; Butchart et al., 2010; Garcia et al., 2011). For example, Garcia et al. (2011) showed that the mean age trend derived from SF_6 over the period 1965–2006 by the Whole Atmosphere Community Climate Model (WACCM) is -0.086 ± 0.011 years decade^{-1}. Efforts are being made to reconcile these discrepancies by reducing uncertainties in both the observational and model estimates, such as those arising from limited observational data of seasonally varying CO_2 mole fractions and unavoidable use of parameterization schemes associated with a coarse model resolution (e.g., Garcia et al., 2011; Stiller et al., 2012; Diallo et al., 2012; Ray et al., 2014).

Given that tropospheric air enters the stratosphere primarily in the tropical tropopause, and that air parcels inside the "tropical leaky pipe" are relatively isolated from mid- and high latitudes by the subtropical mixing barrier (Plumb, 1996; Neu and Plumb, 1999), the mean age is relatively young in the tropical lower stratosphere and the age spectrum takes a compact shape due to transport by slow diabatic vertical advection and very low contributions from the subtropical mixing and diffusion (Plumb and Eluszkiewicz, 1999). The tropical stratosphere is also unique in that the ascending motion is visualized by the water vapor "tape recorder" (Mote et al., 1996). This is independent of mean age since it is an imprint of seasonally varying tropopause temperature on the water vapor mixing ratio in the ascending air masses. All these features make the interpretation of the stratospheric mean age simpler in the tropics as compared to the midlatitudes. Above all, the observations in the tropics are quite limited.

Motivated by these considerations, the Coordinated Upper-Troposphere-to-Stratosphere Balloon Experiment in Biak (CUBE/Biak, Fig. 1.5), a field campaign over Indonesia, was conducted in February to March 2015 (Hasebe et al., 2018, hereafter referred to as H18). CUBE/Biak involved whole air sampling with the aid of balloon-borne cryogenic samplers, radiosondes equipped with ozone, water vapor, and CO_2 son-

des, optical particle counters, cloud particle sensor, and aerosol samplers, along with the continuous operation of aerosol lidar on the ground. Sugawara et al. (2018, hereafter referred to as S18) computed the tropical mean ages from CUBE/Biak SF_6 and CO_2 mole fractions by assuming an age spectrum shape. This data is very new at the moment. Therefore, assessing and understanding the mean ages estimated from this data by a numerical model are necessary.

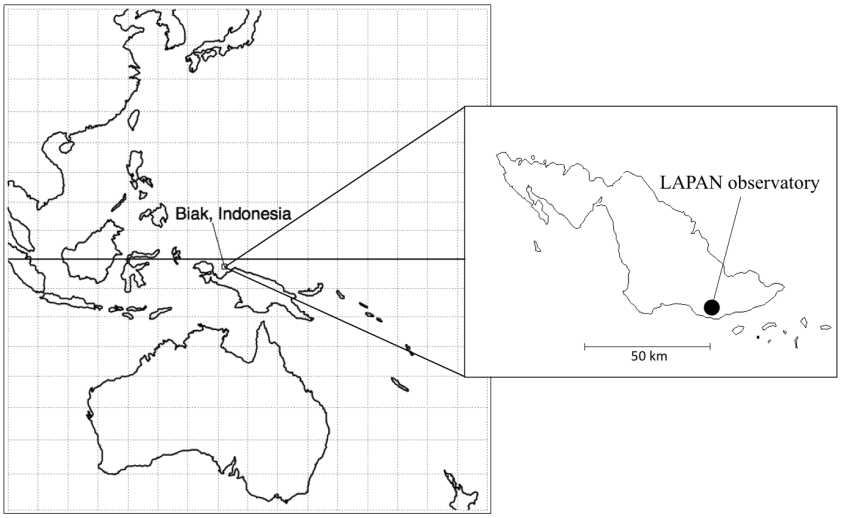

Figure 1.5: Location of Biak station (1.167° S, 136.1° E) and LAPAN observatory. Taken from S18 under a creative commons attribution 4.0 license `https://creativecommons.org/licenses/by/4.0/`.

1.2 Study objective and outline of thesis

This study aims to understand the tropical mean age estimated from CO_2 and SF_6 mole fractions which were obtained from the cryogenic samplers in the CUBE/Biak campaign (S18) by numerical model method. Estimation of mean age from CO_2 and SF_6 observations, with assuming the age spectrum shape as an inverse-Gaussian distribution, might result in an error of mean age. Additionally, requiring a long-term observation of tropo-

spheric CO_2 and SF_6 as reference can lead to unexpected errors in the estimated mean age due to uncertainties of references. With the aid of transport models, the mean age estimated from the BIER method and Lagrangian method are straightforward, do not rely on observation data, and show seasonal variation of the age spectrum. They are also free from assumptions of parameters which are required in the mean age estimation from observations. However, the BIER method is more advantageous than the Lagrangian method. That is because the BIER method makes use the most of a full transport operator in a transport model including parameterization of small-scale transport (unresolved diffusion and mixing). Thus, the BIER method with the aid of an Atmospheric general circulation model-based Chemistry Transport Model (ACTM) (Numaguti et al., 1997), which is nudged to ERA-Interim meteorological fields (Dee et al., 2011), is used in this study.

Estimation of age spectrum from the BIER method calls for releasing artificial pulse tracers at a source region in the troposphere. In model simulations the tropospheric surface (especially the tropical surface) has been commonly chosen as a source region based on the assuming of the well-mixing in troposphere and neglecting the slow ascent of the air in the tropical tropopause layer (TTL) (Fueglistaler et al., 2009; Li et al., 2012a; Ploeger and Birner, 2016; Hauck et al., 2020). It is found that it takes a few weeks up to several months for air parcels to travel from the surface through the TTL (Hall and Plumb, 1994; Strahan et al., 1998; Ray et al., 1999; Park et al., 2007; Chen et al., 2012). However, the TTL is widely recognized as a main gate to the tropospheric air enter the stratosphere; in this manner it is usually considered as the source region when estimating the mean age from observations (Hall and Plumb, 1994). Description of the transport field with the TTL source region in three-dimensional transport models has not been attempted. Through the BIER method, all possible pathways from any source region to any location in the stratosphere can be interpreted. Moreover, since tracers

carry transport histories, the common transport features such as diabatic advections and mixing, can be shown from the distribution of tracers even though the tracer distribution cannot be used to interpret the stratospheric transport, which is apparently due to source and sink dependence of their gradients. Thus, the first objective of this study is to describe stratospheric transport field through the interpretation of the pulse tracer distributions released from the tropical tropopause layer, in addition to release from the tropical surface. The second objective is to apply the BIER method on assessing the tropical mean age, which was estimated from CUBE/Biak data in S18. Additionally, by taking an advantage that the CUBE/Biak mean age was calculated from the Lagrangian method in the ACTM three-dimensional wind field nudged to ERA-Interim reanalysis data in Nguyen et al. (2021, hereafter referred to as Ng21), we compare our results from the BIER method to those from this backward trajectory calculation.

An extended introduction related to stratospheric dynamics and transport is given in Chapter 2 as a background for the discussion in Chapter 5 and Chapter 6. The methods for AoA estimation are described in Chapter 3. Model description and experiment setup are introduced in Chapter 4. Stratospheric transport features through pulse tracer distribution are described and examined in Chapter 5. Chapter 6 shows diagnosis of transport by using the age spectrum and mean age, and validation of the observed mean age in the tropical stratosphere by the BIER and Lagrangian methods. The thesis is wrapped up in Chapter 7 with the major findings of the whole study and an outlook for future research.

Chapter 2

Stratospheric transport and dynamics

2.1 Stratospheric circulation dynamics

Holton (2004) showed a comparison between the meridional distribution of measured temperature and radiatively determined temperature in middle atmosphere (see their Fig. 12.2 and Fig. 12.4). They noticed that the observed temperature is much warmer than the radiatively determined temperature in high latitudes of the winter hemisphere. However, the radiatively determined temperature in the summer pole is warmer than the observed one. Moreover, there is no short-wave heating in the winter polar region due to the absence of sunlight. This leads to a temperature gradient from winter pole to summer pole in the region of 30 to 65 km. Because of the thermal wind balance, westward (eastward) flows in the summer (winter) increase with altitude. Above 65 km, that temperature gradient reverses, leading to a decrease of wind with height in both

winter and summer.

To maintain the observed state of the middle atmosphere, eddy momentum and heat transports play a significant role on driving the flow away from the radiative equilibrium. Thus, the zonally averaged circulations in the middle atmosphere are driven by eddies. In order to understand the role of eddies to the state mentioned above, it is useful to introduce the conventional Eulerian Mean and the Transformed Eulerian Mean.

2.1.1 The conventional Eulerian Mean

Any variable A can be written as the sum of a zonal mean component (denoted by an overbar) and an eddy component (denoted by a prime) at fixed latitude, height and time, i.e., $A = \overline{A} + A'$. Then, equations of zonal-mean zonal momentum, thermodynamic energy, and continuity for quasi-geostrophic theory can be written in the log-pressure coordinate system $z = -H \ln(p/p_0)$ as:

$$\frac{\partial \overline{u}}{\partial t} - f_0 \overline{v} = -\frac{\partial \overline{u'v'}}{\partial y} + \overline{X} \tag{2.1}$$

$$\frac{\partial \overline{T}}{\partial t} + N^2 H R^{-1} \overline{w} = -\frac{\partial \overline{v'T'}}{\partial y} + \frac{\overline{J}}{c_\mathrm{p}} \tag{2.2}$$

$$\frac{\partial \overline{v}}{\partial y} + \frac{1}{\rho_0} \frac{\partial \rho_0 \overline{w}}{\partial z} = 0 \tag{2.3}$$

where $\partial \overline{u}/\partial t$ and $\partial \overline{T}/\partial t$ are the change with time of the zonal momentum and temperature, respectively; $f_0 \overline{v}$ is the Coriolis forcing; $-\partial \overline{u'v'}/\partial y$ and $\partial \overline{v'T'}/\partial y$ are the eddy momentum and heat flux divergences, respectively; $\overline{X}$ is the zonal forcing from the unresolved eddies; $\overline{J}/c_\mathrm{p}$ is the diabatic effects, $c_\mathrm{p} = 1004$ J kg^{-1} K^{-1} is the specific heat at constant pressure, J is the rate of heating per unit mass due to radiation, conduction,

and latent heat release; ρ_0 is the density; $N^2 H R^{-1} \overline{w}$ is the adiabatic cooling, H is a mean scale height ($H = RT/g$), $g = 9.8$ m s^{-2} is the mean magnitude of the gravity acceleration at mean sea level, R is the gas constant for dry air ($R = 287$ J kg^{-1} K^{-1}), N is the buoyancy frequency defined by:

$$N^2 = \frac{R}{H}\left[\frac{\kappa T_0}{H} + \frac{dT_0}{dz}\right]$$

$-dT/dz$ is the lapse rate of temperature. It is positive in troposphere and mesosphere and negative in the stratosphere.

The zonal average of the meridional momentum equation can be approximated by assuming geostrophic balance:

$$f_0 \overline{u} = -\frac{\partial \overline{\Phi}}{\partial y} \tag{2.4}$$

where Φ is geopotential. Combination of this equation with the hydrostatic approximation gives the thermal wind relation

$$f_0 \frac{\partial \overline{u}}{\partial z} + \frac{R}{H}\frac{\partial \overline{T}}{\partial y} = 0 \tag{2.5}$$

This thermal wind balance is destroyed if an ageostrophic mean meridional circulation $(\overline{v}, \overline{w})$ is absent. It is because the eddy momentum and heat flux divergences would tend to change the mean zonal wind and temperature fields. However, small departures of the mean zonal wind from geostrophic balance force a mean meridional circulation so that Eq. (2.5) is maintained. In a stationary flow, the Coriolis force $\approx$ the divergence of eddy momentum fluxes in Eq. (2.1) and the adiabatic cooling $\approx$ the diabatic heating and convergence of eddy heat fluxes in Eq. (2.2). Due to the tendency of cancellation between eddy heat flux convergence and adiabatic cooling, and the diabatic heating being a small residual, the conventional Eulerian mean is not an efficient approach to investigate the

role of eddy forcing in the meridional transport. On the other hand, the transformed Eulerian mean helps to deal with the limitations of this method.

2.1.2 The Transformed Eulerian Mean

The transformed Eulerian mean (TEM) equations can be derived by defined the TEM residual meridional circulation $(\overline{v}^*, \overline{w}^*)$ for quasi-geostropic motions (Holton, 2004):

$$\overline{v}^* = \overline{v} - \frac{R}{\rho_0 H}\frac{\partial\left(\frac{\rho_0 \overline{v'T'}}{N^2}\right)}{\partial z} \tag{2.6}$$

$$\overline{w}^* = \overline{w} + \frac{R}{H}\frac{\partial\left(\frac{\overline{v'T'}}{N^2}\right)}{\partial y} \tag{2.7}$$

By substituting $(\overline{v}^*, \overline{w}^*)$ above into Eqs. (2.1), (2.2), (2.3), we obtain the TEM equations (Holton, 2004) as follows:

$$\frac{\partial \overline{u}}{\partial t} - f_0 \overline{v}^* = \frac{1}{\rho_0}\boldsymbol{\nabla}\cdot\mathbf{F} + \overline{X} \equiv \overline{G} \tag{2.8}$$

$$\frac{\partial \overline{T}}{\partial t} + \frac{N^2 H}{R}\overline{w}^* = -\alpha_r[\overline{T} - \overline{T}_r(y,z,t)] = -\alpha_r \delta\overline{T} \tag{2.9}$$

$$\frac{\partial \overline{v^*}}{\partial y} + \frac{1}{\rho_0}\frac{\partial \rho_0 \overline{w^*}}{\partial z} = 0 \tag{2.10}$$

where $\overline{G}$ is the total zonal force due to large scale and small-scale eddies, $\mathbf{F}$ is the Eliassen-Palm flux (EP flux) which arises from resolved eddies, α is the rate of Newtonian cooling, $\delta\overline{T}$ is difference between zonal mean temperature $\overline{T}$ and its radiative balance $\overline{T}_r$.

If assuming a steady-state condition (no seasonal cycle), the TEM equations show that the Coriolis force due to the residual meridional wind is equal to the eddy

fluxes from both resolved and unresolved eddies. The residual adiabatic cooling is in equilibrium with the diabatic heating. Then, substituting $-f_0\overline{v}^* = \overline{G}$ into Eq. (2.10) with a restriction that $\rho_0\overline{w^*} \to 0$ as $z \to \infty$, we yield

$$\rho_0\overline{w}^* = -\frac{\partial}{\partial y}\left(\frac{1}{f_0}\int_z^\infty \rho_0\overline{G}dz'\right) \tag{2.11}$$

Substituting Eq. (2.11) into Eq. (2.9), we have:

$$\delta\overline{T} = \frac{N^2H}{\alpha_r\rho_0 R}\frac{\partial}{\partial y}\left(\frac{1}{f_0}\int_z^\infty \rho_0\overline{G}dz'\right) \tag{2.12}$$

From Eq. (2.12), we can see that the eddies force the stratosphere away from the thermal equilibrium while the radiation drive it back. Now return to the departure between the observed temperature and the radiatively determined temperature in the middle atmosphere, it is clear that the largest departure from radiative balance occurs in high latitudes in winter stratosphere and in both winter and summer in the mesosphere. The planetary-scale Rossby waves that vertically propagate from troposphere are known as the source of zonal force in the stratosphere. Meanwhile, the breaking of gravity waves, which also propagate from the troposphere into the mesosphere, results in a strong zonal force in the mesosphere.

Considering Eq. (2.8) with an assumption that there is no seasonal cycle, we obtain:

$$-f_0\overline{v}^* = {\rho_0}^{-1}\boldsymbol{\nabla}\cdot\mathbf{F} + \overline{X} \equiv \overline{G} \tag{2.13}$$

f_0 is positive in the winter Northern Hemisphere (NH) and so G is westward force, thus G is negative. Thus, $\overline{v}^* > 0$. By mass continuity, $\overline{w}^* < 0$. In the summer Southern Hemisphere (SH), both f_0 and G are negative. Therefore, $\overline{v}^* < 0$, and thus $\overline{w}^* < 0$. Also by mass continuity, the downward residual motions at the extra-tropics in both

hemisphere must imply a residual upwelling in the tropics (see schematic of residual circulation in Fig. (1.2)).

2.2 Stratospheric transport

The Earth's atmosphere is mainly made up of 78% nitrogen, 21% oxygen and 0.9% argon. All other gases hold the remaining amount with an extremely tiny amount known as tracers. Some tracers are primarily formed in the tropospheric source through (i) processes that occur in nature such as biogenic, the solid Earth, the oceans and in situ formation that forms by chemical reactions in the atmosphere; and (ii) human activities such as fossil-fuel combustion, smogs, and industrial activities. Many of these tracers are observed in the stratosphere. They mostly enter the stratosphere through the TTL. The TTL is the layer of the tropics that lies between 15 – 18 km (World Meteorological Organization, 2007), in which the complex interactions of tropospheric convection, tracers, radiation and stratospheric circulation occurs. Thus, this layer is very important. The TTL varies in altitude and latitude. The coldest temperature ($\leqslant$ 190 K) in the TTL is during the winter Northern Hemisphere (NH). This coldness is reason of dehydration of stratospheric air which firstly observed by Brewer (1949). In the stratosphere, the tracer-included airs are transported by the BDC (Brewer, 1949; Dobson, 1956; Butchart, 2014). The BDC is primary responsibility for the stratospheric transport. The circulation firstly proposed by Brewer (1949) and Dobson (1956) to explain the low mixing ratios of water vapor observed in the stratosphere and high concentration of O_3 observed in the lower polar stratosphere (as O_3 is produced in the tropical stratosphere). As demonstrated in Section 2.1, the BDC is the wave-driven meridional circulation. It contains a persistent shallow branch in the upper troposphere-lower stratosphere (UTLS) in

midlatitudes at each hemisphere driven by synoptic-scale Rossby waves; and a poleward single-cell extended into the middle and upper stratosphere (deep branch) in the winter hemisphere caused by planetary-scale Rossby waves. Dunkerton (1978) showed that the BDC should be considered as a Lagrangian mean circulation and approximated by the TEM residual mean circulation, which equilibrates with the diabatic circulation. The residual meridional circulation is determined by defining a residual stream function, $\overline{\Psi}^*$, from Eq. (2.10) as

$$\overline{v}^* = -\frac{1}{\rho_0}\frac{\partial \overline{\Psi}^*}{\partial z} \qquad ; \qquad \overline{w}^* = \frac{1}{\rho_0}\frac{\partial \overline{\Psi}^*}{\partial y} \tag{2.14}$$

In this study, the BDC is considered as the TEM residual stream function.

A schematic of such TEM residual circulation is illustrated in Fig. 1.2, including the tropical tropospheric and mesospheric residual circulation. In the tropical troposphere, the Hadley cell, which consists of upwelling near the equator and downwelling around 30° latitude in each hemisphere, regimes the transport. A wave-driven single-cell circulation with an upward flow in summer pole heading winter pole dominates the mesosphere. This downward flow penetrates the stratosphere in winter high latitudes and then contributes to the stratospheric transport.

In additional to the BDC, isentropic transport and mixing also play important role to the transport. In wintertime, partly Rossby wave breaking takes place in the midlatitude stratosphere and produces the strongest quasi-horizontal mixing and stirring here, known as "surf zone" (McIntyre and Palmer, 1984) (Fig. 1.2). Such strong mixing flattens the isopleths of mixing ratio of stratospheric tracer in the surf zone (Fig. 1.1). While in the polar vortex, slow diabatic descent tends to press down the isopleths of tracer mixing ratio. The difference in horizontal stirring inside and outside the polar

vortex forms a steep latitudinal tracer gradient at the edge of polar vortex as a barrier to mixing between middle and high latitudes. Like the polar vortex mixing barrier, the subtropical mixing barrier is formed at the edge of subtropic due to the surf zone stirring and the upwelling of BDC in the tropics. These gradients are considered as "transport barriers". The subtropical barrier prevents exchange the air between tropics and midlatitude, while the polar vortex barrier inhibits stirring of vortex air into the surf zone. On the other hand, in the summer hemisphere, due to existence of westward flow, the Rossby wave propagation is mainly blocked (Charney and Drazin, 1961), leading to a silent summer. Therefore, the isopleths of tracer mixing ratio have small slopes from the subtropical region to high latitudes. Although the subtropical mixing barrier is found in the summer hemisphere, mechanism of its formation has not yet been understood well. In fact, the transport barriers are not perfect. This is because it is found evidences of transport of tropical air into the winter surf zone (Randel et al., 1993) and of vortex air into middle latitudes (Plumb, 2007).

In the midlatitude UTLS, there is a small-scale two-way mixing caused by the descend of BDC and tropospheric intrusions into stratosphere through the tropopause. The tropopause is the transition layer between the troposphere and stratosphere (solid line from north to south in Fig. 1.2). It is established at levels from 7 –10 km in polar latitudes and from 16 – 18 km in the tropical region. Its height is not fixed, but varies with time and latitude. It had been indicated that the seasonal variation of tropical tropopause is driven by extratropical pumping (Yulaeva et al., 1994). As a result, the tropopause is higher in summer and lower in winter, implying seasonal variation of two-way exchange between troposphere and stratosphere. The thermal tropopause is defined as "the lowest level at the lapse rate decreases to 2 K km^{-1} or less, provided also the average lapse rate between this level and all higher levels within 2 km does not exceed 2 K km^{-1}" by the World Meteorological Organization (WMO) (World Meteorological

Organization, 1995). The place in which the removal of tracers out of atmosphere is known as sink region.

Chapter 3

Estimation of the age spectrum

3.1 Introduction

As mentioned in Chapter 1, the BIER method which incorporates the effects of small-scale mixing of air on transport is employed to explore the stratospheric transport field. Moreover, since the mean age estimated from the BIER method is compared with that estimated from observations by S18 and from the Lagrangian method in Ng21, the description of these methods is also stated in this Chapter.

3.2 Age spectrum and mean age of air

A mathematical formulation of the age spectrum was first presented by Hall and Plumb (1994). The continuity equation for a passive and inert tracer's mixing ratio χ, which is

conserved following the motion, is represented in the form:

$$\frac{\partial \chi}{\partial t} + \mathscr{L}(t) = 0 \tag{3.1}$$

where $\mathscr{L}$ is the linear differential transport operator. A boundary condition on a known time-varying mixing ratio, $\chi(\Omega, t^{'})$, which applied at a specific Ω (e.g., the Earth's surface or tropical tropopause layer), is propagated into the stratosphere via the transport operator $G(\boldsymbol{r}, t|\Omega, t^{'})$. The general solution at any stratospheric point $\boldsymbol{r}$ and time t for Eq. (3.1) is

$$\chi(\boldsymbol{r}, t) = \int_{-\infty}^{t} \chi(\Omega, t^{'}) G(r, t|\Omega, t^{'}) dt^{'} \tag{3.2}$$

$G(\boldsymbol{r}, t|\Omega, t^{'})$, the Green's function, propagates concentration at Ω, past time $t^{'}$ when the tracer had ended connection with Ω to the point $\boldsymbol{r}$ at field time of interest t, and thus it is called the boundary propagator (Waugh and Hall, 2002). By introducing the transit time $\tau \equiv t - t'$, Eq. (3.2) reduces to

$$\chi(\boldsymbol{r}, t) = \int_{0}^{\infty} \chi(\Omega, t - \tau) G(\boldsymbol{r}, t|\Omega, t - \tau)\ d\tau. \tag{3.3}$$

Eq. (3.3) shows that $G(\boldsymbol{r}, t|\Omega, t - \tau)\ d\tau$ is the mass fraction of air at $(\boldsymbol{r}, t)$ that had last been in contact with Ω between τ and $\tau + d\tau$ ago. In other words, $G(\boldsymbol{r}, t|\Omega, t - \tau)$ specifies the distribution of transit times or the age spectrum (Hall and Plumb, 1994). In this sense, t and t' are called the field time and source time, respectively. By definition, the mean age Γ is estimated as the first moment of the age spectrum:

$$\Gamma = \int_{0}^{\infty} \tau G(\boldsymbol{r}, t|\Omega, t - \tau) d\tau \tag{3.4}$$

The spectral width (spread) is often denoted by Δ defined as follows:

$$\Delta = \sqrt{\frac{1}{2}\int_0^\infty (\tau - \Gamma)^2 G(\boldsymbol{r}, t|\Omega, t-\tau) d\tau} \tag{3.5}$$

3.3 Methodologies

3.3.1 Boundary impulse evolving response method

The age spectrum is a boundary propagator $G(\boldsymbol{r}, t|\Omega, t-\tau)$ introduced in the form of a Green's function (Section 3.2). It could be estimated from the response $\chi(\boldsymbol{r}, t)$ by setting the tracer mixing ratio at the source region as a "pulse" at transit time $\tau = \tau_i$ (≥ 0), i.e., by substituting the Dirac delta function $\delta(\tau - \tau_i)$ for $\chi(\Omega, t-\tau)$ in Eq. (3.3):

$$\begin{aligned}\chi(\boldsymbol{r}, t) &= \int_0^\infty \delta(\tau - \tau_i) G(\boldsymbol{r}, t|\Omega, t-\tau)\ d\tau \\ &= G(\boldsymbol{r}, t|\Omega, t-\tau_i).\end{aligned} \tag{3.6}$$

Eq. (3.6) can be interpreted as a function of τ_i (≥ 0) for a fixed $(\boldsymbol{r}, t)$, and $\chi(\boldsymbol{r}, t)$ is referred to as the boundary impulse response (BIR) (Haine et al., 2008; Li et al., 2012a). In practice, $\delta(\tau - \tau_i)$ is approximated by the mixing ratio of an inert pulse tracer $\chi(\Omega, t-\tau_i)$ released at the source region Ω at the source time $t - \tau_i$. The principle of this method is schematically illustrated in Fig. 3.1a.

This method was modified by implementing multiple pulse tracers with different source time $t - \tau_i$ in a single transport calculation (BIER method) making it possible to estimate the time-dependent age spectrum efficiently (Ploeger and Birner, 2016). In each of our experiment, at each single source region, 62 one-month pulses are introduced

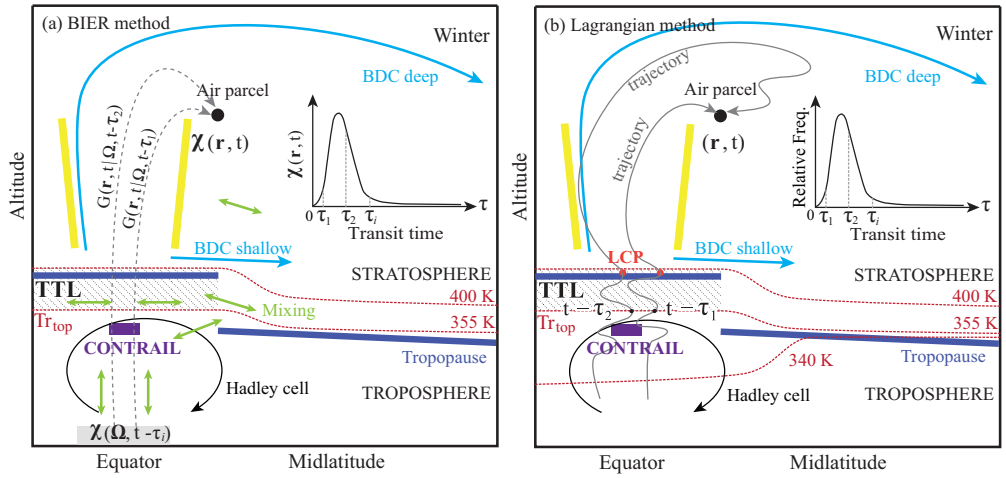

Figure 3.1: Schematic illustration of the concept of the age spectrum at a location $\boldsymbol{r}$ and time t calculated by (a) Boundary Impulse Evolving Response (BIER) and (b) Lagrangian backward trajectory methods. Thick yellow lines show the the subtropical mixing barriers. Hatched area shows the tropical tropopause layer (TTL). $\chi(\boldsymbol{r}, t)$ is the mixing ratio at $(\boldsymbol{r}, t)$. $\chi(\Omega, t - \tau_i)$ is the mixing ratio at the source region Ω (shaded area) at the source time $t - \tau_i$. Dashed arrows illustrate the propagation from the source region to stratospheric air parcel by the boundary propagator $G(\boldsymbol{r}, t|\Omega, t-\tau_i)$ in the BIER method. Solid wavy arrows are the trajectories in the Lagrangian method, in which the count of transit time commences with the last passage through 355 K isentrope. The inset represents the shape of the age spectrum at $(\boldsymbol{r}, t)$. The location of CONTRAIL observations used as the upper tropospheric reference record in the estimation from observations is depicted in purple area. Figure is taken from Ng21.

as $\chi(\Omega, t - \tau_i)$ (section 4.2), creating 62 BIRs. These BIRs will build a BIR map for a point $\boldsymbol{r}$ with horizontal and vertical axes corresponding to the source time and field time, respectively. The age spectrum at $\boldsymbol{r}$ is the horizontal cut of the BIR map backward in source time at the field time t.

3.3.2 Lagrangian backward trajectory method

In the Lagrangian method, the age spectrum is estimated independently from the BIER method. This method is conceptually much easier than the BIER method to estimate the age spectrum at an any given point. By contrast, in order to obtain picture of global

distribution of the age spectrum, the BIER is much easier and saves more storage and more CPU time. In backward trajectory calculation, a huge number of air parcels is initialized at particular times and height ranges wherein CUBE/Biak data was sampled (see Table 3 in H18). Kinematic backward trajectories are calculated by tracking the position of air parcels advected by the three-dimensional wind. Then, the age spectrum is estimated by counting the transit time τ during the advection along each kinematic trajectory since the last passage through the top of the tropical troposphere ($\mathrm{Tr_{top}}$) (Fig. 3.1b). In Ng21's analysis, $\mathrm{Tr_{top}}$ was taken to be the 355 K isentropic surface referring to the fact that the influence of tropical convective motion almost ceases at this level and diabatic forcing gradually changes to radiative heating in and above the TTL (Hasebe and Noguchi, 2016). Calculations were terminated when the trajectories reach the bottom (ground surface) and the top (1 hPa pressure level) boundaries.

3.3.3 Estimation of observational age of air

The mole fractions of CO_2 and SF_6 derived from the air samples taken from the CUBE/Biak campaign over Indonesia are used to estimate the mean age of air. The overall uncertainties of the observed mole fractions are 0.1 μmol mol^{-1} for CO_2 and better than 0.09 pmol mol^{-1} for SF_6, leading to possible errors in the mean age of 0.3 to 0.4 years for CO_2 and 0.4 to 0.5 years for SF_6. See S18 for the details of the preprocessing of collected samples. For this estimation, the age spectrum, having been assumed to take the form of the inverse-Gaussian distribution (Waugh and Hall, 2002),

$$G(\tau;\Gamma,\Delta) = \sqrt{\frac{\Gamma^3}{4\pi\Delta^2\tau^3}}\exp\left(-\frac{\Gamma(\tau-\Gamma)^2}{4\Delta^2\tau}\right) \tag{3.7}$$

is sought to reproduce the observed mole fraction of the corresponding species by sweeping the parameter Γ. This function is known as the solution of the continuity equation for linearly increasing tracers in a one-dimensional diffusive system (Hall and Plumb, 1994). While only one value (mole fraction) is known, the other parameter Δ is assumed to be given by Γ through the relationship $\Delta^2/\Gamma = 0.7$ years. This value, called the ratio of moments, is suggested by Hall and Plumb (1994) from the results of a stratospheric GCM and is found to give the best overall agreement between SF_6-derived and CO_2-derived mean ages in the northern mid- and high latitude stratosphere (Engel et al., 2002). Then the mole fraction at time t, derived by substituting Eq. (3.7) together with known tropospheric values $\chi_0(t)$ into Eq. (3.3),

$$\chi(t;\Gamma,\Delta) = \int_0^\infty \chi_0(t-\tau)G(\tau;\Gamma,\Delta)\ d\tau, \tag{3.8}$$

is compared with observations, and the parameter Γ that gives the best match to the observation is adopted as the observational estimate of the mean age (S18). The tropospheric reference was derived from direct measurements of air samples collected by the Comprehensive Observation Network for TRace gases by AIrLiner (CONTRAIL) program (Machida et al., 2008; Sawa et al., 2008; Matsueda et al., 2015) in the tropical upper troposphere within the area 5° S – 5° N and 142° E – 150° E at an altitude of 10 – 13 km (purple area in Fig. 3.1).

3.4 Correction of age spectrum tail

The first moment of age spectrum strongly depends on its tail. However, as the transport calculations cannot last for an infinite length of time, the integration must be truncated at some finite length, which leads to underestimation of the mean age. To overcome

this, a tail correction has been applied (e.g., Hall et al., 1999; Reithmeier et al., 2008; Li et al., 2012a; Ploeger and Birner, 2016). The age spectrum tail partly has an exponential decay after 3-5 years in the lower stratosphere (Ehhalt et al., 2004; Diallo et al., 2012; Ploeger and Birner, 2016). Following Ploeger and Birner (2016), an exponential function was fitted to each age spectrum derived from the transport calculations and the obtained decay rate, ξ, is used to extrapolate the age spectrum after its truncation to infinity. In this calculation, the decrease of the age spectrum is taken after 4th year at everywhere. Due to different lengths of integrated period of each pulse release in this study (section 4.2), the age spectra are truncated at different transit time thresholds, τ^*. To compute ξ, only the age spectrum values at the transit times of consecutive years after the first four years (4 years $< \tau < \tau^*$ years) are used. The decay rate is estimated at each grid point. The corrected age spectrum at $(\boldsymbol{r}, t)$ are calculated by:

$$G(\boldsymbol{r}, t|\Omega, t-\tau) = \begin{cases} G(\boldsymbol{r}, t|\Omega, t-\tau) & \tau \leq \tau^* \\ G(\boldsymbol{r}, t|\Omega, t-\tau^*) e^{-\frac{\tau-\tau^*}{\xi}} & \tau > \tau^* \end{cases} \tag{3.9}$$

Then corrected mean age (Γ_{corr}) and the corrected width (Δ_{corr}) are respectively estimated by

$$\Gamma_{\text{corr}} = \int_0^{\tau^*} \tau G(\boldsymbol{r}, t|\Omega, t-\tau) d\tau + G(\boldsymbol{r}, t|\Omega, t-\tau^*)\xi(\tau^* + \xi) \tag{3.10}$$

$$\begin{aligned} \Delta^2_{\text{corr}} = \frac{1}{2}\Bigg(& \int_0^{\tau^*} (\tau - \Gamma_{\text{corr}})^2 G(\boldsymbol{r}, t|\Omega, t-\tau) d\tau \\ & + \xi\Big[(\tau^* - \Gamma_{\text{corr}})^2 + 2\xi(\tau^* - \Gamma_{\text{corr}} + \xi)\Big] G(\boldsymbol{r}, t|\Omega, t-\tau^*)\Bigg) \end{aligned} \tag{3.11}$$

This correction is also applied to the results from the Lagrangian method. Throughout this study, Γ_{corr} and Δ_{corr} are presented.

Chapter 4

Application of a general circulation model to the diagnosis of stratospheric transport field

4.1 ACTM description

The ACTM used in the present study is an online version and developed by the Center for Climate System Research/National Institute for Environmental Studies/Frontier Research Center for Global Change (CCSR/NIES/FRCGC) atmospheric general circulation model (AGCM) (Numaguti et al., 1997; Patra et al., 2009). It is configured as in Ishijima et al. (2010) to have 67 sigma (σ) levels from the surface to a height of approximately 90 km, with the horizontal resolution in T42 spectral truncation (equivalent to $\sim 2.8^\circ \times 2.8^\circ$ latitude–longitude gridpoints). The vertical resolution is 0.5 km inside the TTL, and ~ 0.9 km in the main stratosphere. The cumulus convection parameterization

scheme is the simplified Arakawa and Schubert scheme (Arakawa and Schubert, 1974; Numaguti et al., 1997). The adjusted cloud mass flux is used to calculate the updraft and downdraft due to cumulus convection. Gravity wave drag is calculated by a scheme of McFarlane (1987). Influence of gravity wave on the stratospheric circulation in this and newer version of ACTM was discussed in detail by Patra et al. (2018). For the calculation of tracer transport, it applies a 4th order flux-form advection scheme using a monotonic Piecewise Parabolic Method (PPM) (Colella and Woodward, 1984) and a flux-form semi-Lagrangian scheme (Lin and Rood, 1996). The second-order vertical eddy diffusion scheme of Mellor and Yamada with cloud effects (Mellor and Yamada, 1982; Numaguti et al., 1997) is applied for sub-grid-scale vertical fluxes of meridional velocity, temperature and mixing ratios of tracers. This model has been used in studies of the transport properties of chemical constituents such as SF_6 (Patra et al., 2009), N_2O (Ishijima et al., 2010) and in demonstrating the utility of a novel three-dimensional transport formulation (Kinoshita et al., 2019).

4.2 Experiment design

In the present study, realistic runs are made by nudging the horizontal winds and temperature towards those of the ERA-Interim with the relaxation time of 2.4 hours at 6-hour time intervals from 1 January 2000 to 31 March 2015. Sea ice and sea-surface temperature (SST) fields are also supplied from the ERA-Interim at 6-hour time intervals. The first five years (January 2000 to December 2004) are regarded as the spin-up period and excluded in the following analysis. For the ozone field for radiative calculations, 6 hourly full-resolution model level data up to 1 hPa from the ERA-Interim (Dragani, 2011), and above 1 hPa from United Kingdom Universities' Global Atmospheric Modelling Pro-

gramme (UGAMP) ozone climatology (Li and Shine, 1999) are used.

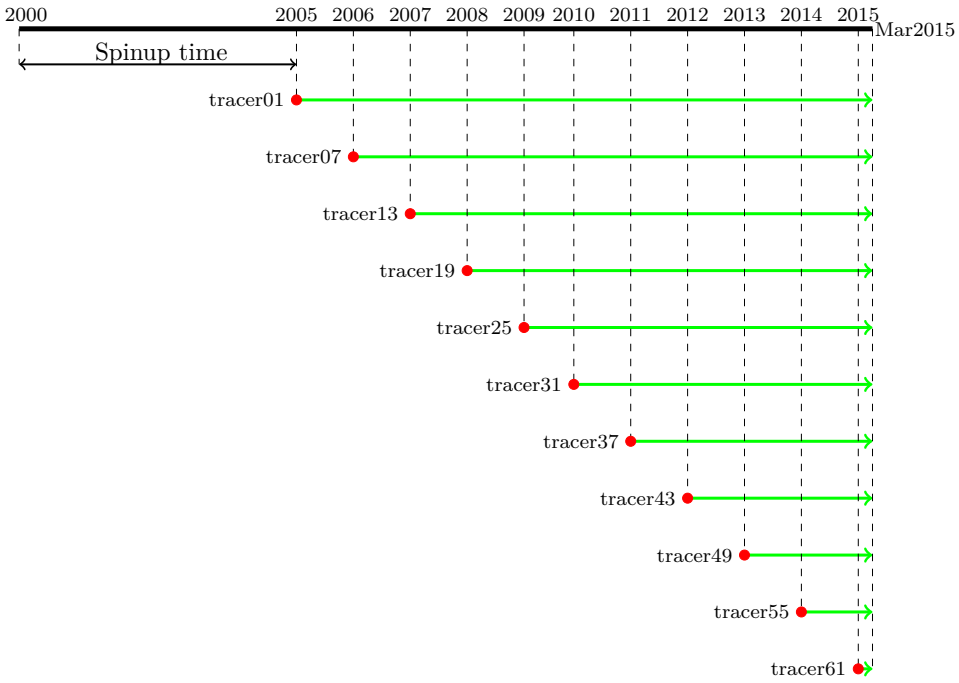

Figure 4.1: Schematic of the BIER simulations. Length of color arrows including red and green shows the integrated time of tracers released in, for example, Januaries. Red represents the source time (i.e., tracer released at the first month). Green represents the integration time (no pulse release).

The estimation of the age spectrum following the BIER method (section 3.3.1) requires many temporal pulses simulations at different source times at a specified source region Ω. In this study, two experiments are made. The first one is with Ω placed at the tropical surface corresponding to in latitude band 15° S–15° N and in the lowest level of model. Another one is with Ω placed at the TTL covering from 30° S–30° N and 355 K–400 K. Both experiments, every single pulse tracer is released at Ω by setting their mixing ratio to a constant value (1 ppbv) for a month (pulse tracer). The releases are made in odd-numbered months; i.e., January, March, May, July, September, and November of each year throughout the simulation period (January 2005 to March 2015, see Fig. 4.1), resulting in release of 62 distinct tracers for the tropical surface source

and of another 62 distinct tracers for the TTL source. The instantaneous release from a single source region and the chemically conservative properties of tracers help simplify the diagnosis of the transport field simulated by the model. Output data are monthly mean mixing ratio value.

One-hour averaged values of wind field simulated by ACTM nudged to the ERA-Interim was used at one-hour intervals in calculating of the backward trajectory in Ng21. Note that Ng21 showed that using the wind field from ACTM nudged to ERA-Interim improved the values of mean age to be closer with observations in comparison with using the winds from ERA-Interim. Fig. 9 in Ng21 showed the tropical upwelling speed in ERA-Interim is faster than that in ACTM nudged to ERA-Interim, but is slower than that ACTM free running. An animation in Supplementary in Ng21 provides imagines in backward-in-time movement of air parcels in the stratosphere among these three cases.

Chapter 5

Diagnosis of stratospheric transport by pulse tracer experiments

5.1 Introduction

Since the variations in the zonal direction is quite small in the stratosphere, especially in the tropics, in this Chapter we focus our analysis on zonal-mean field. Moreover, the scope of this study concentrates in the aspects of stratospheric transport. Thus, the spatial variations of tracer in the two source regions (the tropical surface and the TTL) and at some levels in the troposphere are shown in Appendix.

5.2 Releases from the tropical surface

Considering the strong seasonality of the stratospheric circulation, we examine the zonal-mean distribution and local rate of change of January (July)-released pulse tracers during

February (August) and March (September) of the first year (i.e., next two months) and February (August) and March (September) of the second year (i.e., 13th and 14th month since release) to describe the stratospheric transport features in particular. The analyses are made by taking average the tracers released on the same calendar month but in different years from 2005 to 2013 (e. g., January 2005, January 2006, January 2007, and so on).

Figure 5.1 (top panels) shows the latitude-height distributions of the simulated pulse traces in February of the first year (i.e., the second month) on the left and March of the first year (i.e., the third month) on the right panels since release, respectively, and the tendency of the tracer field (ppbv month^{-1}) estimated by the difference between February and March on the middle. The curves in white are the contours of the TEM residual stream function, $\overline{\Psi}^*$, averaged for the same period 2005–2013 using ERA-Interim analyses. During the second month from release (Fig. 5.1(a)), the tracer is transported vertically to the upper troposphere and horizontally toward high latitudes by the tropospheric Hadley circulation from the source region assigned from 15° S–15° N in the lowest model level in January. Due to the deflection to the summer (Southern) hemisphere of the ascending branch of the Hadley circulation, the tracers are primarily trapped inside the winter (Northern) hemispheric Hadley cell. Some amount of the tracer is transported to the TTL and the lower stratosphere (LS). In the third month of tracer release (March), the intrusion of the ascending branch of the Hadley cell to the Southern Hemisphere (SH) is narrowed toward the equator. Although a large amount of the tracer is still confined to the tropospheric Hadley cell especially in the spring (Northern) hemisphere, some portion of the tracer is pumped up to the TTL and LS in this month (Fig. 5.1(c)). Stratospheric concentrations above the 400 K isentrope in the subtropics and in the lowermost stratosphere at mid- and high latitudes are higher in the winter hemisphere than in the summer hemisphere, suggesting a stronger circulation

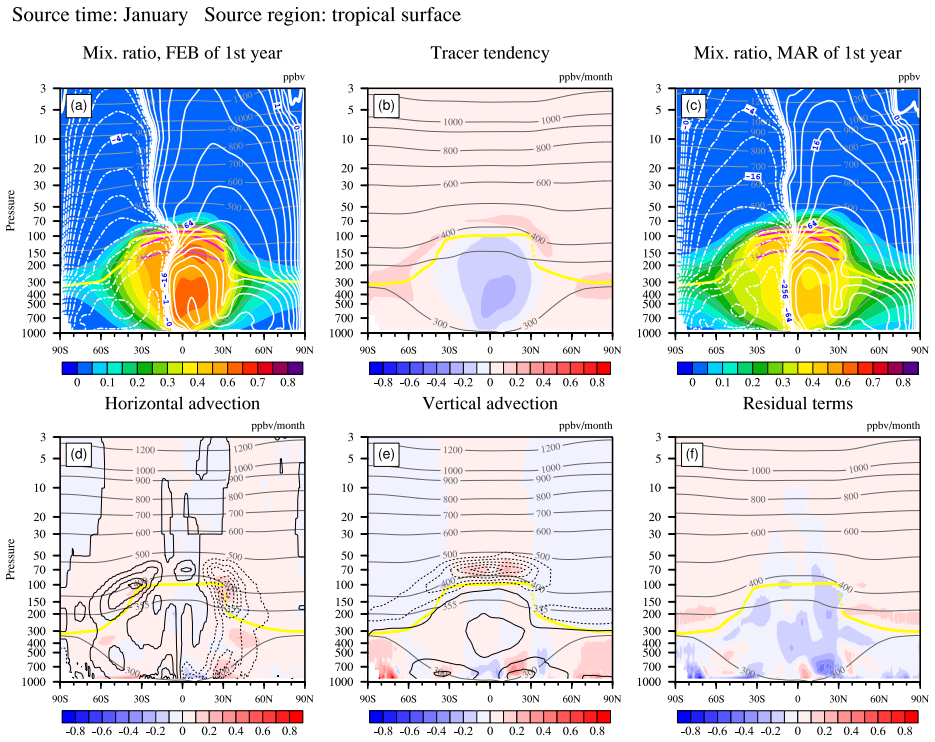

Figure 5.1: Monthly mean distributions of surface-released pulse tracer (ppbv) for (a) the second month (February) and (c) the third month (March) from release, while (b), (d), (e) and (f) respectively show the tendency of tracer mixing ratio during the two-month period between (c) and (a), horizontal advection, vertical advection and remaining terms (ppbv month^{-1}). Black lines are the horizontal (d) and vertical tracer gradients (e), respectively, in solid for positive and dashed for negative values. The contour interval is 3×10^{-8} ppbv m^{-1} for horizontal and 3×10^{-5} ppbv m^{-1} for vertical gradient. Zero lines are omitted. Grey lines are potential temperature (K). The dotted yellow line is the tropopause position (WMO-defined). Area covered by the purple lines represents the TTL. White curves (solid for positive and dashed for negative values) show the Transformed Eulerian Mean (TEM) residual stream function (kg m^{-1} s^{-1}) estimated from the ERA-Interim. The value of contours after 0 line is respectively $0.125^n (n = 0, 32768)$. (a) is taken from Ng21.

towards the winter pole.

To understand the transport features responsible for redistributing the tracers, the continuity equation for the pulse tracer is considered. The local rate of change of the zonal mean tracer mixing ratio $\overline{\chi}$, is described by the zonally averaged continuity equation expressed as follows in the TEM framework (Andrews et al., 1987, Eq. (9.4.13))

$$\frac{\partial \overline{\chi}}{\partial t} = -\overline{v}^* \frac{\partial \overline{\chi}}{\partial y} - \overline{w}^* \frac{\partial \overline{\chi}}{\partial z} + \frac{1}{\rho_0} \boldsymbol{\nabla} \cdot \mathbf{M} + P - L. \tag{5.1}$$

where $(\overline{v}^*,\ \overline{w}^*)$ are the TEM residual velocities, the overbar indicates a zonal mean, $\mathbf{M}$ is the TEM eddy flux vector, and P and L are the chemical sources and sinks, respectively.

Fig. 5.1(b) shows the local rate of change of the mixing ratio between February and March (left-hand side of Eq. (5.1), while those in (d) and (e) show the contribution from the first and the second terms, respectively, of the right-hand side of this equation. Panel (f) shows the residual of all the other terms, corresponding to the sum of eddy transport, unresolved small-scale mixing, and source/sink terms. We can see negative values in the tropical troposphere while positive values in the extratropical troposphere and the LS. The tropospheric decrease shows a peak in the tropical lower troposphere. The stratospheric increase is found in the lowermost stratosphere exhibiting some anisotropy between the hemispheres. In the SH, the increase is found to the south of 30° S and some intrusion to the troposphere along the isentropes $\sim$ 300 K is noticeable. In the NH, on the other hand, the increase is found in the tropics and subtropics above 400 K isentropic surface in addition to that around 300 K north of 60° N. As for the decrease in the tropical middle troposphere, the contribution from the residual terms (Fig. 5.1(c)), probably coming from unresolved convective transport, plays a role. The increase in midlatitude troposphere (Fig. 5.1(b)) is not well represented by quasi-isentropic eddy mixing due possibly to the mixture of unresolved convective mixing into the resolved

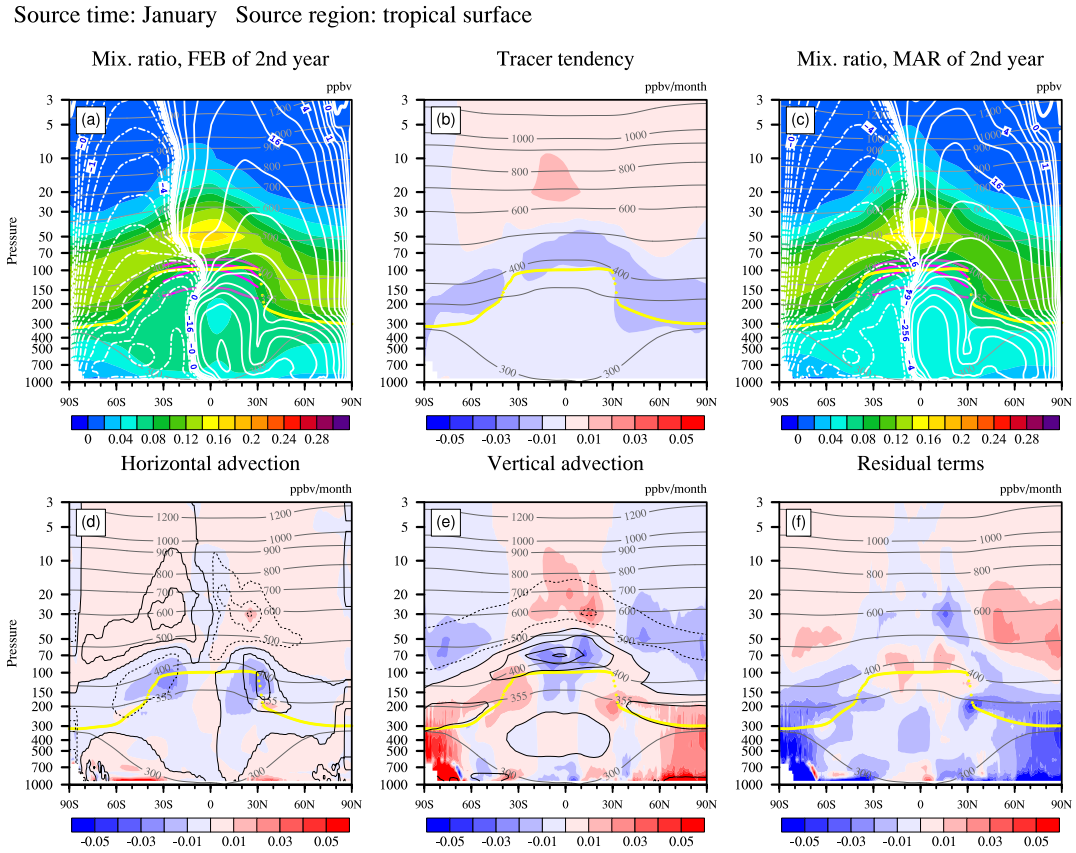

Figure 5.2: The same as Fig. 5.1 but for the distribution one year later. That is, tracer distributions after (a) 14 and (c) 15 months from release and (b) monthly tendency between the two months. Note that the color scale is different from Fig. 5.1. The contour interval is 1×10^{-8} ppbv m^{-1} for (d) and 1×10^{-5} ppbv m^{-1} for (e). (a) is taken from Ng21.

eddy mixing (Fig. 5.1(f)). In the TTL and the tropical LS, the increase is brought about by the upward transport by mean circulation. The maximum in the lower-stratospheric northern subtropics is achieved by the combination of the horizontal and vertical advection. On the other hand, the increase in the extratropical LS is a result of the eddy transport.

As the tracer distribution is mostly confined below the lowermost stratosphere during the first few months from the surface release, the tracer field has little sensitivity to

the stratospheric circulation. To examine the transport features in the stratosphere, the tracer distributions and the associated tendency one year after those shown in Fig. 5.1 are illustrated in Fig. 5.2. We can see the concentration of surface-released tracers is deeply transported into the stratosphere (particularly in the tropics). A tropical maximum at around 500 K isentrope ($\sim$ 50 hPa) indicates that a part of the tracers that were widespread in the TTL one year earlier (Fig. 5.1) are pumped up into the tropical stratosphere. At the same time, some tracers, having leaked from the tropical pipe, are transported to the extratropics by quasi-isentropic mixing to create lower-stratospheric maxima in mid- and high latitudes. The altitude and sharpness of the maximum reflect the strength of the extratropical suction pump and permeability of the subtropical mixing barrier. The lower-stratospheric maxima, taking a value of > 0.12 ppbv in the mid- and high latitudes, are found at higher isentropic levels in the Southern Hemisphere, as a result of the seasonal and hemispheric anisotropy of both the shallow and deep branches of the BDC. The tendency appears positive (negative) above (below) $\sim$ 500 K isentrope except for Southern high latitudes, although the magnitude is small (less than ± 0.02 ppmv month^{-1}). Associated with the redistribution of tracers in one year, the contribution of horizontal advection in the subtropical tropopause region and the vertical advection in the tropical LS turns from positive (Fig. 5.1(b)) to negative (Fig. 5.2(b)). The stratospheric increase takes maximum in the tropics of the SH due partly to the vertical advection, whereas the wide-spread increase in the extratropics is mainly driven by the horizontal transport from the tropics. The decrease in the Southern high latitudes is brought about by poleward and downward advection. In the extratropical LS, the contribution of the residual terms (probably eddy mixing) also changes sign from positive to negative. The decrease is most pronounced along 355 K isentrope in the Northern mid-latitudes probably reflecting the decreasing tendency in the tropical upper troposphere.

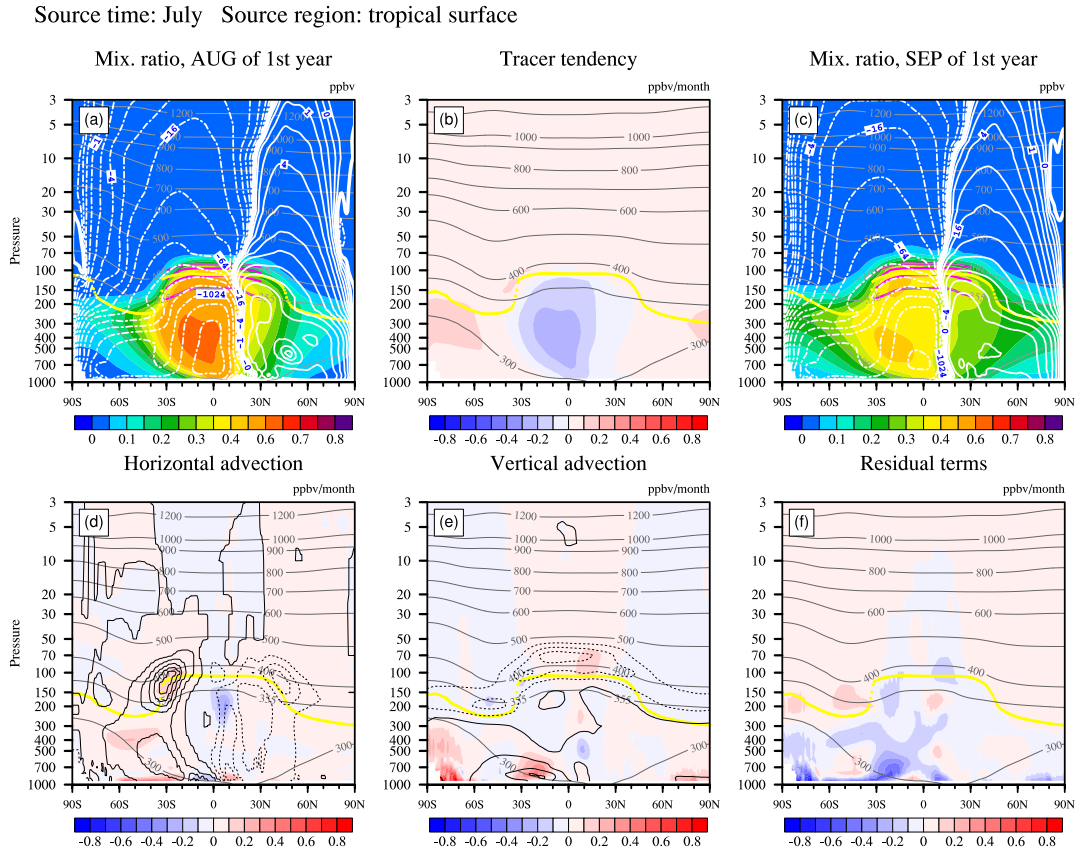

Figure 5.3: The same as Fig. 5.1 but for the tracers release in July. The second and the third months are August and September, respectively.

In view of the strong seasonal variation in the TTL and the LS together with the marked asymmetry in the wave-driving between the two hemispheres, it is important to conduct similar analysis in Northern summer. Figures 5.3 is the same as Fig. 5.1 but for the surface tracers released in July. Generally the distribution in the second (August) and the third (September) month and the tendency in-between of the July-released tracers (Fig. 5.3) are similar to those released in January if the latitude is reversed. The tropospheric concentration tends to be smaller in the case of July release than in January release due possibly to the larger tropospheric volume (higher tropopause indicated by yellow dots in Figs. 5.3) in the southern high latitudes. Note that due to the unique temperature profile in polar winter, with the minimum temperature location within

the lower stratosphere, the thermal tropopause defined by WMO cannot be correctly determined. The role of mean motion and the eddies (Fig. 5.3(f)) looks qualitatively similar.

The stratospheric transport features are examined by looking at similar figures at one year later (Fig. 5.4). As compared to the release in January, we can see in the case of July release the shape of mixing ratio isopleths is analogous (if latitudes are turned around), although the stratospheric concentrations are smaller and the transport speed is slower. This will be understood by the hemispheric asymmetry in the strength of the stratospheric wave-pumping in winter. There exists a difference in the contribution of the horizontal advection, negative in the NH (Fig. 5.2(d)) while positive in the SH (Fig. 5.4(d)), in the lowermost stratosphere of the winter hemisphere.

The descriptions mentioned above show faster propagations in the extratropics, at least at the source times in January and July in comparison with those simulated in Chemical Lagrangian Model of the Stratosphere (CLaMS), which is also nudged to ERA-Interim and shares the same source region at the tropical surface (Ploeger and Birner, 2016). This is possible due to too fast meridional mixing in the ACTM (Patra et al., 2018).

The transport features shown above are limited to those of tracers released in January and July. To assess the time evolution of tracer fields, examples of the BIRs are investigated. Fig. 5.5 shows simulated BIR maps over the equator, 50 hPa and at 80° N, 100 hPa created by 62 tracers released at the tropical surface from January 2005 to March 2015. At 50 hPa in the equator, tracer concentrations tend to be high during the wintertime. In addition, there are intermittent higher peaks shown as orange and red spots at (t', t) = (March 2007, October 2007) and (November 2009, July 2010). In these cases, the transit zone of the pulse tracers, that is, the tropical lower stratosphere

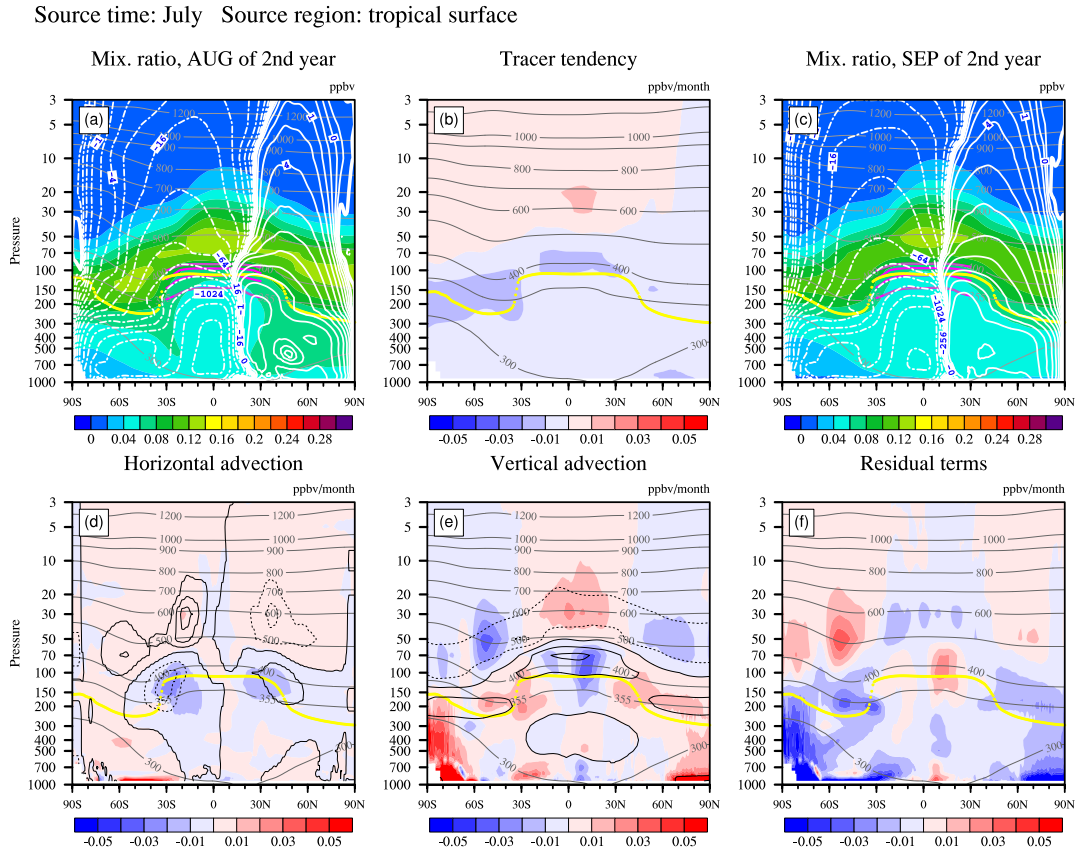

Figure 5.4: The same as Fig. 5.2 but for the tracers release in July. The second and the third months are August and September, respectively.

below 50 hPa, is mostly covered by easterly shear in the zonal wind (Fig. 5.6). This means that the upward tracer transport driven by extratropical pumping is intensified by the secondary circulation associated with the equatorial quasi-bienien oscillation (QBO) (Plumb and Bell, 1982; Baldwin et al., 2001). Thus, as discussed by Ploeger and Birner (2016), the higher peaks of the BIR map occur where the QBO facilitates seasonal intensification of the wave-driven pumping from the northern midlatitude stratosphere. By contrast, at 80° N, 100 hPa, the seasonal variation of BIRs is rather clear. The high concentration is found in summer and early autumn in the NH associated to the tracers released in winter-spring. The summer-released tracers show weak peaks due to restraining of the polar vortex barrier in winter.

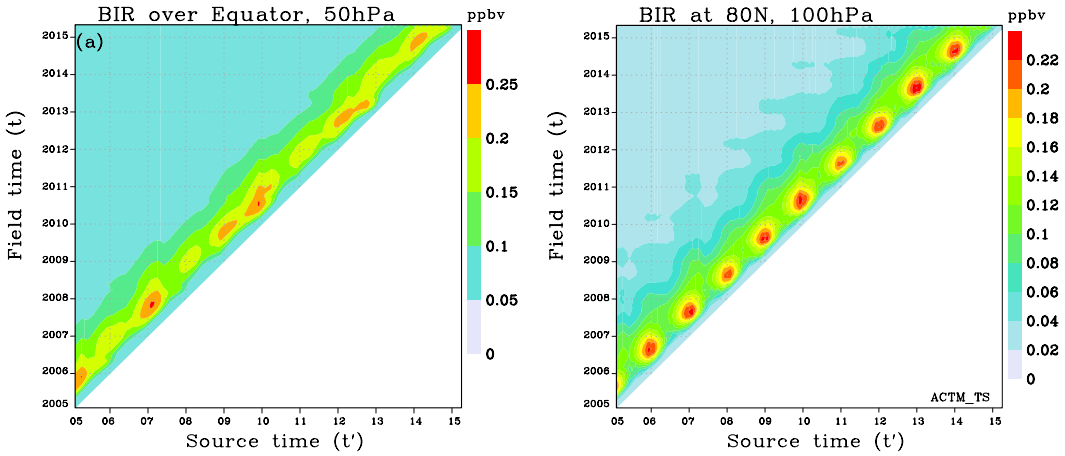

Figure 5.5: BIR map over the equator at 50 hPa and at 80° N, 100 hPa

The inter-annual variation is examined through the temporal evolutions of January- and July-released pulse tracers at some representative altitudes and latitudes. For convenience, we denote the temporal evolutions of January- and July-released pulse tracers as the January- and July-BIRs, respectively. Since the coverage of our transport calculation is limited to $\sim$ 10 years from January 2005 to March 2015, we show the five-year time-series of tracers by taking the average of those released in January (red) and July (blue) of 2005, 2006, 2007, 2008, and 2009. The values are scaled so that the

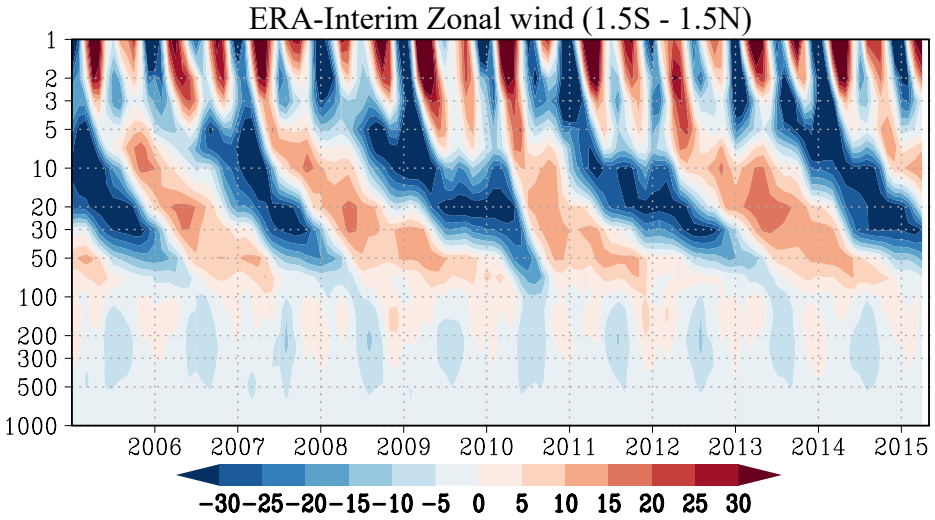

Figure 5.6: A time-height section of mean zonal wind (m s^{-1}) over the equator.

BIRs express the probability distribution function (PDF) to be used in the mean age estimation (Section. 3.3.1). Figure 5.7 shows the PDF over the equator (the average of two BIRs at 1.4° N and S), 20.9° N, 46.0° N and 79.5° N at 100 hPa, 50 hPa and 10 hPa pressure levels. The shading surrounding the thick lines are the five-year range between the maxima and minima. In the tropics, the BIR-peaks appear earlier and higher for the tracers released in January than in July on 100 hPa. However, this is not always the case for the 50 and 10 hPa levels. Upon the passage of westerly (easterly) wind shear associated with the quasi-biennial oscillation (QBO) in the lower stratosphere below these levels, the accompanying descending (ascending) motion will bring about later (earlier) BIR peaks (see Ploeger and Birner (2016)). The BIR at 50 hPa over the equator reaches a maximum several months after release. At 10 hPa, the transit time of about two years necessary for the surface tracers to reach a maximum agrees well with that in Li et al. (2012b) (see their Fig. 1 (top)), although the decay time appears longer in the present study. Sufficient mixing and recirculation occurs higher up at 10 hPa. Rapid isentropic mixing explains part of the widening of the age spectrum, explaining contributions from air parcels with large transit times due to back and forth recirculation between the tropical pipe and the midlatitudes. The latitudinal variation of the BIRs on 50 hPa shows a tendency for peaks to be later and smaller and the decay time to be longer at higher latitudes. The seasonal dependency of our results at 20.9° N on 50 hPa agrees with that at 20° N on the 420 K isentrope ($\sim$ 70 hPa) in Li et al. (2012a). That is, the January-BIR shows an earlier and higher peak than the July-BIR. These results agree with previous studies and are consistent with our current knowledge indicating that the AGCM realistically time-interpolates the discrete ERA-Interim wind data and simulates dynamical–physical processes of tracer transport reasonably well.

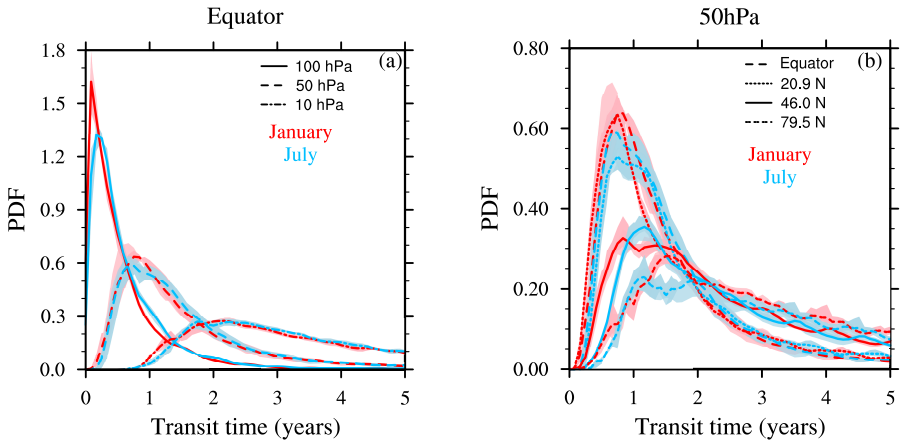

Figure 5.7: Evolution of January (red) and July (blue) BIRs on (a) 100, 50, and 10 hPa over the equator and (b) 50 hPa at 20.9, 46.0 and 79.5° N. The thick lines are the average of five BIRs for tracers released from 2005 to 2009, while the shading shows the BIR range among the five releases. The unit is year^{-1}. Figure is taken from Ng21.

5.3 Releases from the tropical tropopause layer

The transport calculations similar to those shown in the previous section are repeated by setting the source region to the TTL. The results are shown in Fig. 5.8. During the three months since the one-month tracer release in the source region (30° S – 30° N and 355 K – 400 K), the tracer is gradually transported upward in the tropics and poleward and downward in the extratropics, and widely distributed in the LS of both hemispheres. The subtropical maxima of tracer in the second month from release (Fig. 5.8(a)) suggests a rapid transport by the shallow branch of the BDC. The transport by the residual circulation brings about the lower-stratospheric increases more enhanced in the NH due to poleward advection in the midlatitudes and upward motion in the tropics (Fig. 5.8(d, f)).

In the TTL, while the general decrease follows the pulse-shaped release in the source region, the enhanced decrease around its flanks (Fig. 5.8(b)) is attributable

to the horizontal advection and the isentropic mixing between mid- and low latitudes (Fig. 5.8(d, f)). The large decrease associated with the poleward motion (Fig. 5.8(d)) and

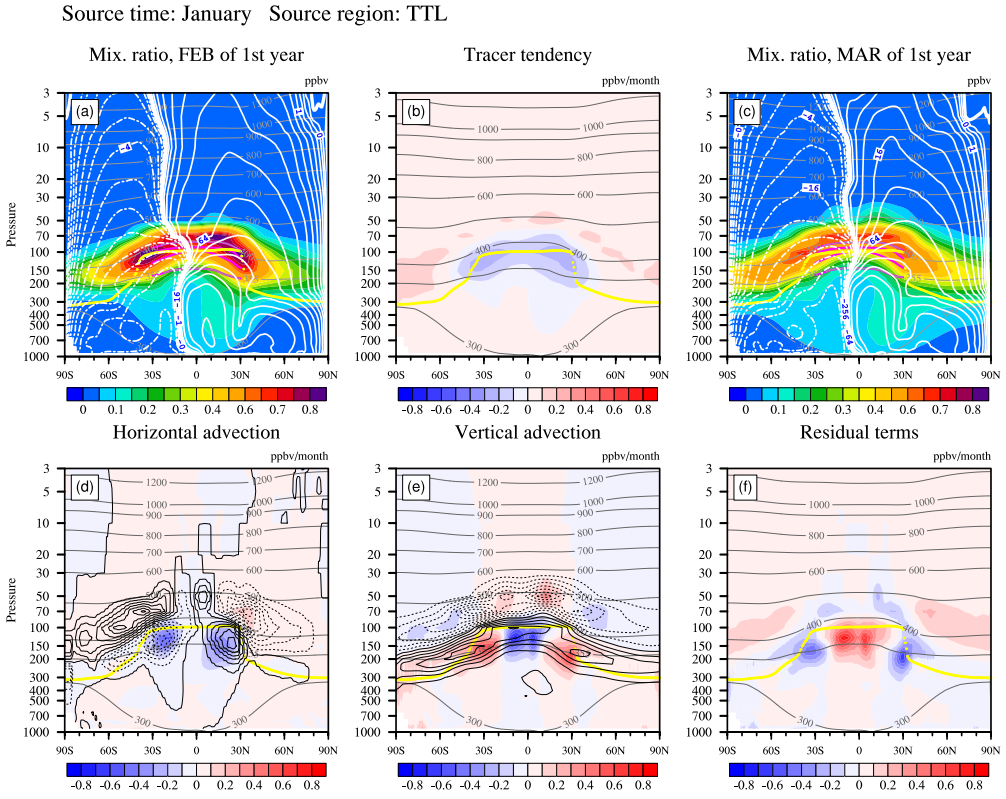

Figure 5.8: Monthly mean distributions of pulse tracer (ppbv) released at the TTL for (a) the second month (February) and (c) the third month (March) after January release, while (b), (d), (e) and (f) respectively show the tendency of mixing ratio during the two-month period between (c) and (a), horizontal advection, vertical advection and remaining terms (ppbv month^{-1}). Black lines are the horizontal (d) and vertical tracer gradients (e), respectively, in solid for positive and dashed for negative values. The contour interval is 3×10^{-8} ppbv m^{-1} for horizontal and 3×10^{-5} ppbv m^{-1} for vertical gradient. Zero lines are omitted. The dotted yellow line is the tropopause position. Area covered by the purple lines represents the TTL. White curves (solid for positive and dashed for negative values) show the TEM residual stream function (kg m^{-1} s^{-1}) estimated from the ERA-Interim. The value of contours after 0 line is respectively $0.125^n (n = 0, 32768)$.

the large decrease (increase) associated with the upward (downward) motion (Fig. 5.8(e)) appear quite reasonable. However, the quasi-mirror image of the residual term (Fig. 5.8(f)) against vertical advection near the bottom of the TTL (355 K) is rather hard to under-

stand. A possible interpretation may be that the eddy mixing tends to compensate for the variations due to mean transport at the bottom of the TTL. As the tracer concentration is available only on a monthly basis, however, further analysis is not attempted here.

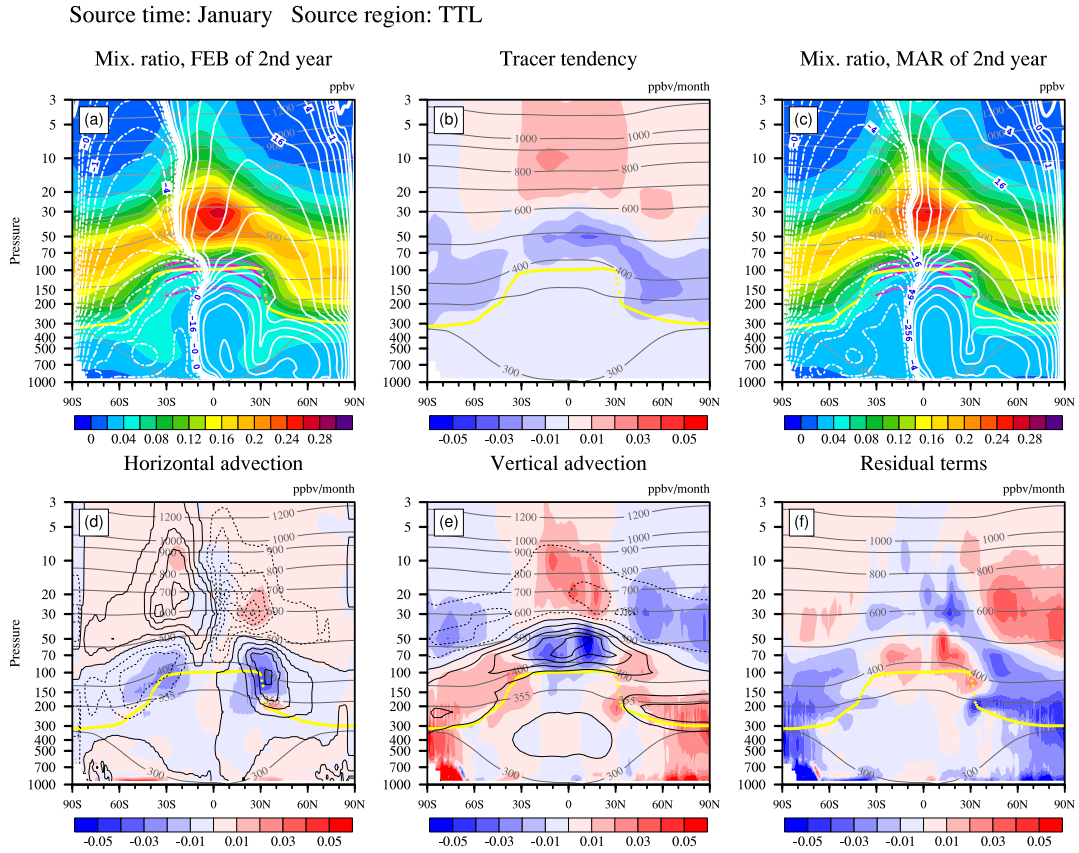

Figure 5.9: The same as Fig. 5.8 but for the distribution after (a) 14 and (c) 15 months from January release and (b) monthly tendency between these two months. The color scale is different from Fig. 5.8. The contour interval is 1×10^{-8} ppbv m^{-1} for (d) and 1×10^{-5} ppbv m^{-1} for (e).

The tropospheric variations are characterized by decreases along the descending branch of the Hadley circulation and an increase in the remaining part of the troposphere (Fig. 5.8(b)). The former is brought about by the transport by residual circulation. As the descending branch of the Hadley cell is stronger in the winter (Northern) than in

the summer hemisphere, more amount of the tracers descend in the NH than in the SH troposphere.

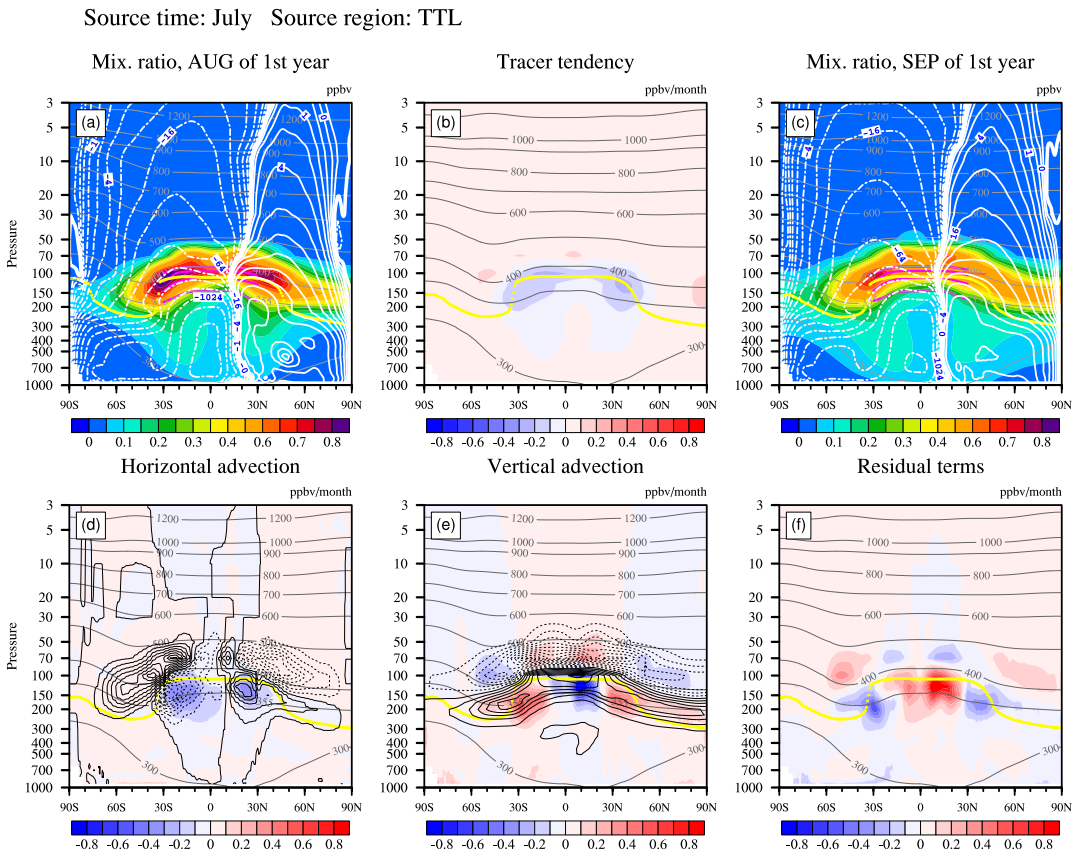

Figure 5.10: The same as Fig. 5.8 but for tracers released in July. The second and the third months are August and September, respectively.

Illustrations similar to those shown in Fig. 5.8 but those one year later are shown in Fig. 5.9. The features of tracer distributions are qualitatively similar, but the maximum concentrations are higher and located in higher altitudes in the case of TTL release (Fig. 5.9) than in the surface release (Fig. 5.2). The distribution of the tendency is slightly shifted upward in the case of TTL release. These features are expected if we consider the difference in the distance from the source regions.

The seasonal asymmetry appears most clearly in the lower-stratospheric tracer

distributions in winter. The tracer concentration in the polar lower stratosphere in winter is much smaller in the case of July release (Fig. 5.10) than in January release (Fig. 5.8). This is interpreted as the weaker eddy transport (panel (f) of Figs. 5.8 and 5.10) across the mixing barrier of the polar vortex in the Southern than in the Northern hemisphere.

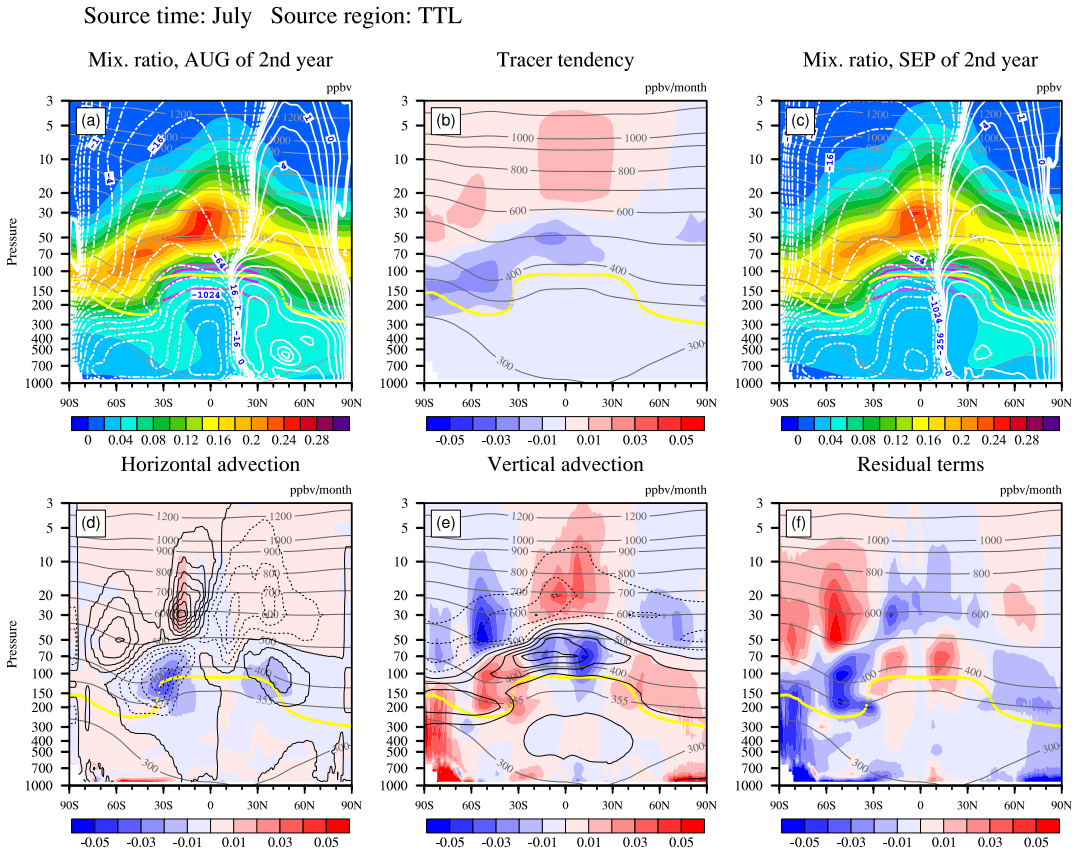

Figure 5.11: The same as Fig. 5.9 but for tracers released in July. The second and the third months are August and September, respectively.

After one year, the hemispheric asymmetry no longer exists and we can see the tracer concentrations more abundant in the Southern (Fig. 5.11) than in the Northern (Fig. 5.9) lower stratosphere in winter. It is interesting to see that the contribution of downward transport (Fig. 5.11(e)) just outside the southern polar vortex is reversed due

to the reversal of the vertical concentration gradient at around 70 hPa (Fig. 5.11) and that it is mostly compensated by the effect of eddy transport (Fig. 5.11(f)). Unlikely the releases at the surface, the releases at the TTL show a much higher mixing ratio.

The time development of tracers released at the TTL is shown in Fig. 5.12. They are partly alike to the surface release, except the transit time to the lower stratosphere and tropical region is a few months shorter. Moreover, the bimodal shape of January BIRs at 46° N and 50 hPa is unclear. At 79.5° N, 50 hPa this shape is found for both January- and July-BIR.

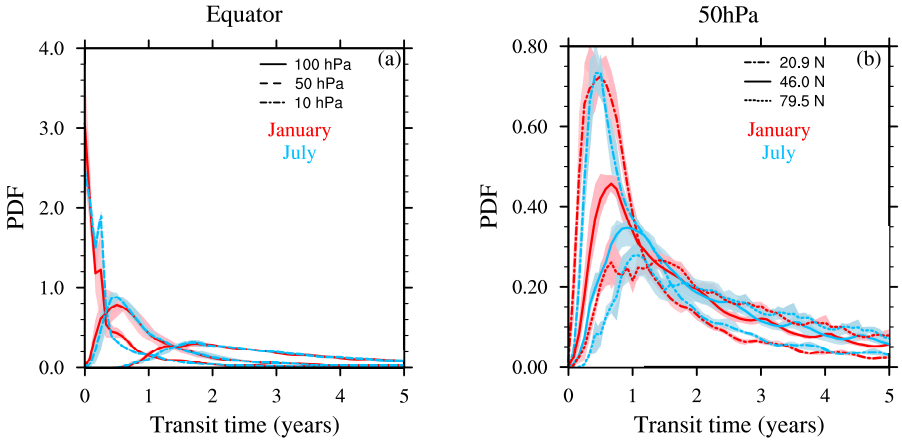

Figure 5.12: The same as Fig. 5.7 but for tracers released in the TTL.

5.4 Comparison between tropical surface- and TTL-releases

It is readily expected that the stratospheric AoA, if defined by the elapsed time since release, is older in the case of surface release than that of TTL release depending on the finite length of time necessary for the surface air to reach TTL. However, there is

no guarantee that the time lag appears uniformly in the whole stratosphere due to the transport features both in the troposphere and the stratosphere. The following features that appear as the difference in the distribution of pulse tracers described in the previous sections are important for the purpose of studying the influence of source region setting (either on the tropical surface or in the TTL) on the stratospheric AoA in the BIER method. The descriptions are focused on the stratospheric features referring to those of TTL-released tracers relative to the surface-released tracers.

The tendency of the stratospheric tracer concentrations during Northern spring (February to March) is characterized by the increase in the lowermost stratosphere of the Southern high latitudes and the Northern subtropics in the case of surface-released tracers (Fig. 5.1(b)). These features appear almost the same in the TTL-released tracers (Fig. 5.8(b)) except that the tendency in the tropical lowermost stratosphere is negative due to simulation setting.

Transport features related to the difference in the tracer distributions having been brought about by the source region setting are recapped as follows.

1. The stratospheric transport field in Northern spring (February to March):

    - There found a rapid transport toward high-latitude lowermost stratosphere of both hemispheres due to eddy mixing with the air in the upper troposphere (Fig. 5.1(f)). During the early days since release from the surface, a part of the increase in high-latitude stratosphere is brought about by a direct quasi-isentropic mixing with mid- and high latitude troposphere, which is not well-captured by the simulation by TTL-release.
    - The tropical ascending motion spans widely between 30° N and S of the equator bounded by the subtropical mixing barrier.

- The shallow branch of BDC transports lower-stratospheric air from the tropics to the extratropics of both hemispheres in a way more effective to the Northern (winter-spring) hemisphere.
- The summer polar stratosphere (south of 70° S as a whole) is characterized by the decrease with an enhancement in the lower stratosphere due to the downward transport by mean circulation.

2. The stratospheric transport field in Southern spring (August to September):

   - The rapid poleward transport in the lowermost stratosphere of both hemispheres appears also in Southern spring.
   - The tropical ascending motion appears a little narrower in width but enhanced in strength over the equator.
   - The lower-stratospheric transport due to the shallow branch of BDC is more intense in the Southern (winter) hemisphere. This hemispheric asymmetry appears more pronounced in the difference field. After one year, the decreasing tendency in the Northern lower stratosphere is smaller in the surface-released tracer field (Fig. 5.4(b)) than in the TTL-released tracer field (Fig. 5.11(b)).

Generally, the stratospheric transport features are reasonably represented irrespective of the choice of the source region. However, the bottom of the high-latitude stratosphere especially during the early days from release is differently sensitive to local eddy mixing, either with the midlatitude lower troposphere (surface release) or with the upper troposphere (TTL release).

Chapter 6

Diagnosis of stratospheric transport using the age of air

6.1 Introduction

In chapter 5, we showed the stratospheric transport features through the temporal and spatial distribution of tracers released at the tropical surface and the TTL. Further, in this chapter, before applying the BIER method in assessing the tropical mean age estimated from CUBE/Biak CO_2 and SF_6 data, we investigate the stratospheric transport features through the global distributions of age spectrum and mean age of air. Due to its seasonal variation as well as its wide coverage in latitude and height, considering the TTL as a single source region appears inappropriate. Thus, in this chapter, we only represent the age spectrum and mean age calculated from releases assigned at the tropical surface.

6.2 Global distribution of age spectrum and mean age

Figure 6.1 shows the zonal distribution of January and July age spectrum, averaged over 3 years (2012–2014), at 100 hPa, 50 hPa and 10 hPa in the stratosphere for the tracers released at the tropical surface. Due to application of the extension of the age spectrum tail, it allows to present the tails for 10-year transit times. At 100 hPa ($\sim$ 400

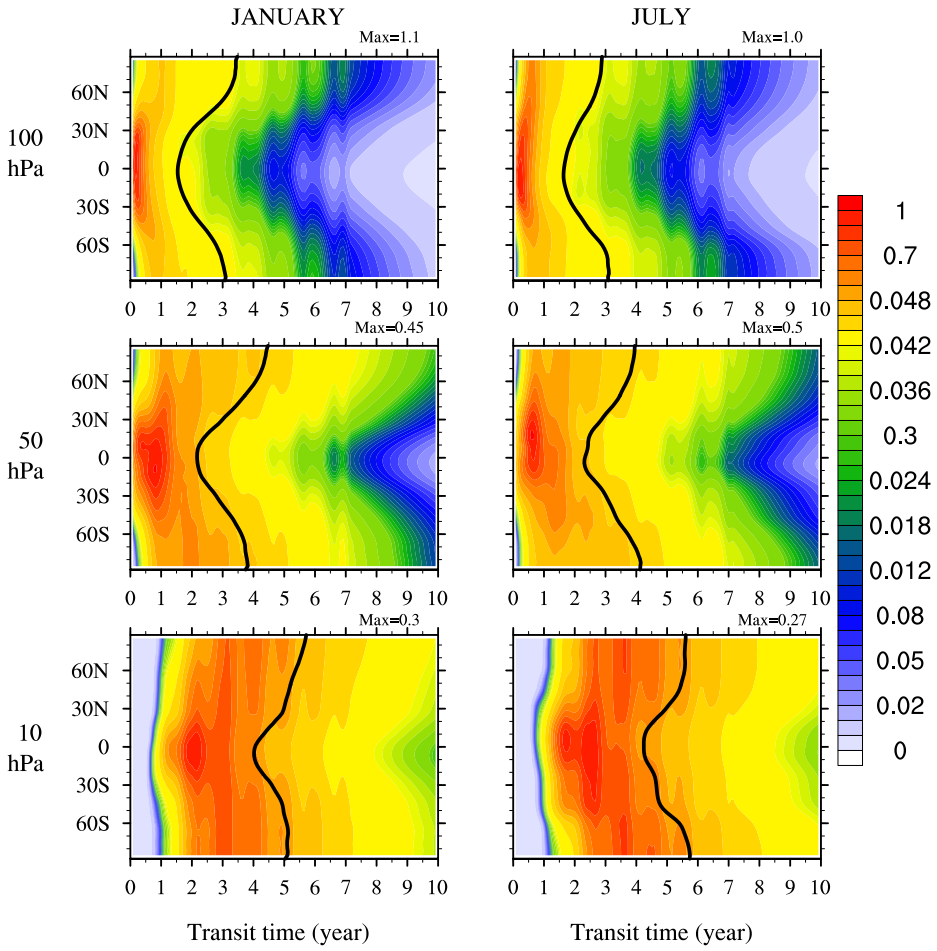

Figure 6.1: Age spectrum (PDF) in January (left) and July (right) at 100 hPa, 50 hPa, 10 hPa estimated for tracers released at the tropical surface. The black line is Γ_{corr}.

K), the age spectra are quickly decreased in the tropics along with a clear and very young peak in both January and July. As the modal age represents the time scale of the most common pathway, the youngest modal ages around 1 – 2 months indicates that the tracers released at the tropical surface are quickly transported to the top of the TTL. These youngest modal ages are shifted toward the winter hemisphere, consistent with faster upwelling of the BDC in this time. A slightly younger mean age in the Northern winter than in the Southern winter is a result of the stronger upward motion of the BDC in the Northern winter. In extratropics, particularly in the winter hemisphere, the age spectra show long tails with weakly multiple peaks caused by the annual cycle of the recirculation, the seasonality of mixing barriers and of the stratospheric shallow branch consistent with previous studies (e.g., Reithmeier et al., 2008; Li et al., 2012a; Ploeger and Birner, 2016). Young tropical air is mixed well into extratropical region by quasi-isentropic motion (Fig. 5.2 and Fig. 5.4) in the summer. The mean age is older in the LS NH winter than in the LS SH winter. It suggests a stronger quasi-horizontal transport in the SH winter in comparison to the NH winter. The decrease of age spectrum becomes slower with increase of latitude and altitude. At 50 hPa ($\sim$ 500 K) surface, effects of the transport features on the age spectrum at 50 hPa are generally similar to those at 100 hPa. However, the multiple peaks appear not only in high latitudes, but also obviously seen in the tropics. The width of modal age in the July age spectrum is significantly narrower than that of January, leading to the tropical stratospheric mean age in July is older than in January. They result from the seasonalities of not only the upward motion of BCD, but also the QBO around 50 hPa – 30 hPa levels (Fig. 5.6). The interannual variation of QBO also has an impact on the tropical age spectrum at 10 hPa. The January age spectra at 10 hPa have annually repeating peaks at long transit time ($\sim$3, 4 years) caused by westerly QBO phase (Ploeger and Birner, 2016). At high latitudes, the modal ages are found at transit time of 3, 4 and 5 years not only in the NH winter

but also in the NH summer due to the descending motion along the deep branch of the BDC. The old peaks in the NH summer suggest an important role of recirculation of the extratropical old airs back to tropics during this season. Very similar features are found for the July age spectrum (right-hand-side panels of Fig. 6.1). The age spectrum with multi-peaks simulated by ACTM nudged toward ERA-Interim generally represents a good agreement with that simulated by the CLaMS model with the same meteorological field in Ploeger and Birner (2016), although the multi-peaks in the low latitudes are not shown in Li et al. (2012a).

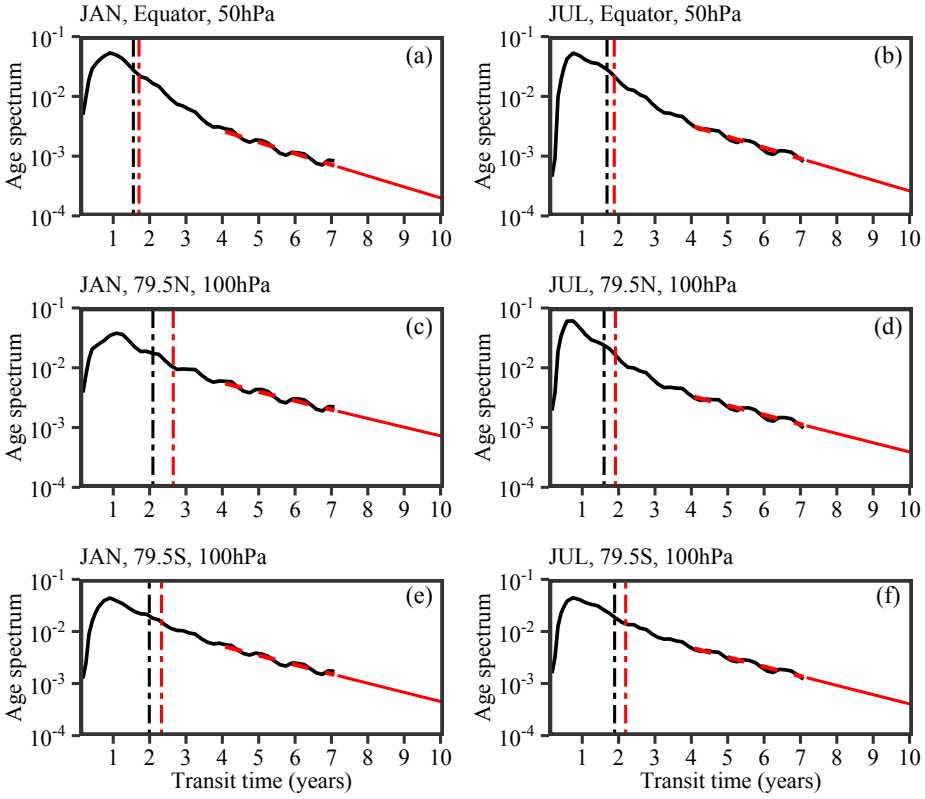

Figure 6.2: Multi-year averaged age spectrum (month^{-1}) at (top) 50 hPa over the equator, and at 100 hPa (middle) 79.5° N, and (bottom) 79.5° S in January (left) and July (right). The solid black lines show the age spectra. The decay rate of the age spectrum estimated by the least square fit between 4 to 7 years is used for tail correction applied to the transit time longer than 4 years (red line). The vertical dot-dash lines show the mean age with (red) and without (black) tail correction.

Since the limitation of calculation storage, the tail of age spectrum is corrected. The correction creates longer tails. Li et al. (2012b) showed that more than 50 % of the mean age comes from the tail. As a result, the corrected mean age, Γ_{corr}, is older than the original simulated age. Figure 6.2 shows the single age spectra over the equator and 79.5° N and S in the lower stratosphere for the case of tracers released in the tropical surface. In January, Γ_{corr} is several weeks older than the uncorrected mean age at 50 hPa over the equator and more than a half year older at 100 hPa at 79.5° N. In the high-latitude stratosphere, both uncorrected and corrected mean ages are older in January than in July. The spectral peak, which is independent of the tail correction, appears later in January than in July, despite the earlier emergence of BIR peaks in January than in July in the equatorial stratosphere at 50 hPa (Fig. 5.7). It is obvious that the individual BIR and age spectrum of pulse tracer are totally different in unstable flow (Haine et al., 2008).

Figure 6.3 represents the meridional distribution of mean age in January, March, May, July, September and November corresponding to months of source time for tracers released at the tropical surface. In the tropical troposphere where the source region is setup, the mean age is youngest. The mean age at the source region is not zero because air after leaving is recirculated and brought back old air. The rest of troposphere, the mean age is a bit older than in the tropics due to quasi-horizontal mixing with old air of stratosphere from midlatitudes. In the stratosphere, the distribution of mean age is exactly following the structure of BDC. The mean age is young in the tropics in the upwelling regime of BDC and becomes older with increasing latitude and altitude. It is easy to see the signals of transport barriers, quasi-horizontal mixing in the wintertime and early spring through sharp gradients and flattened isopleths in the midlatitudes. They are clearer in the SH (e. g., July, September) than in the NH (e. g., January, March). In the high-latitude upper stratosphere, the mean age is oldest. It indicates the

importance of the deep branch of BDC on the transport.

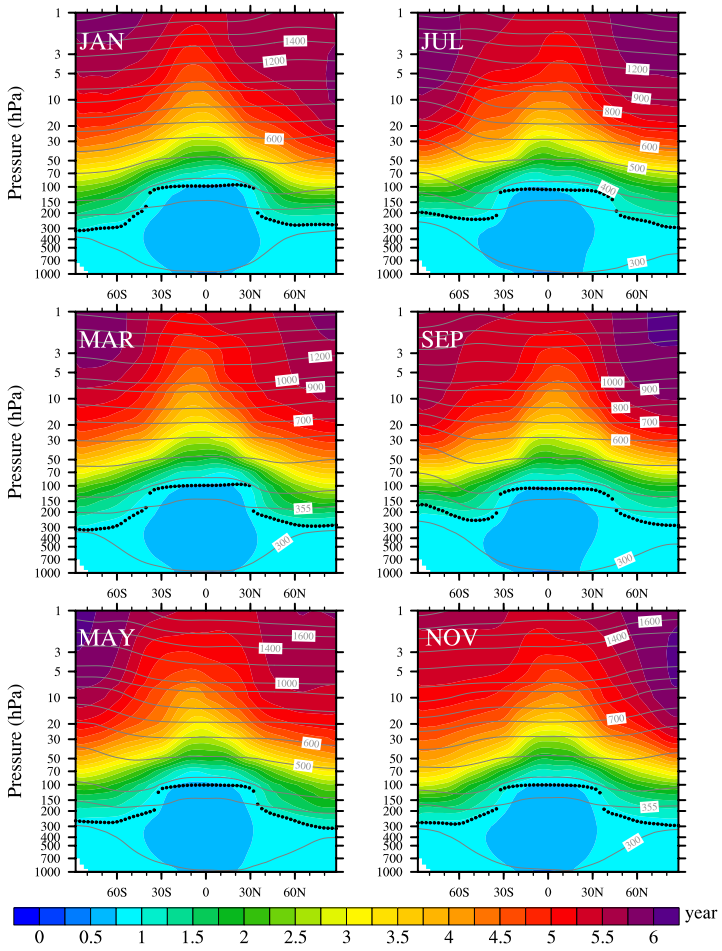

Figure 6.3: Zonal mean distribution of three-year averaged mean age in January, March, May, July, September and November at the tropical surface release.

To further evaluate performance of the ACTM simulation, the seasonal mean Γ_{corr} estimated from the tracers released in the tropical surface is compared with that of Ploeger and Birner (2016) since the simulation design, the method of tail correction, and the use of ERA-Interim meteorological fields in this study mostly follow those of them. Fig. 6.4 represents the latitude–height section of Γ_{corr} in winter and summer. The structure of distribution of mean age is exactly following the movement of Brewer-Dobson circulation. That is, the age is young in tropics due to the upward flow of circulation.

On the other hand, it becomes older when going towards higher latitude related to the transport of deep branch. In comparison with Fig. 4 in Ploeger and Birner (2016), there is good agreement in overall features including the seasonal asymmetry between the hemispheres, strong latitudinal gradient associated with the subtropical mixing barriers, small slope of contours in high-latitude LS in the summer hemisphere, and so on. However, there are some quantitative differences at high latitudes. In the case of the December–January–February (DJF) average, for example, the 4.5-year contour lies above the 650 K and 500 K surfaces at 90° S and 90° N, respectively, in Fig. 6.4, while it lies below 500 K and 450 K, respectively, in Ploeger and Birner (2016), indicating that the mean age is younger by about 0.5 to 1.0 year in our ACTM. The younger age also appears in the June–July–August (JJA) average over Antarctica. This tendency is recognized from the AoA inter-comparison of global transport models; the ACTM nudged to Japanese 25-year Reanalysis (JRA-25; Onogi et al., 2007) horizontal winds and temperature showed the strongest convective mixing in the tropics and the youngest air at the high-altitude poles amongst the models that participated in the comparison (Krol et al., 2018). Such an overall underestimation of the mean age in mid-to-high latitudes is also consistent with the description of fast horizontal transport of the ACTM in section 5.2. Despite this issue and the availability of only 3 years (2012–2014) for estimating the multi-year age spectra, the overall agreement is encouraging. In the following section, we employ the BIER method with the source region at the tropical surface to estimate the mean age in the equatorial lower stratosphere intending to interpret the observational estimates given by the cryogenic air sampling.

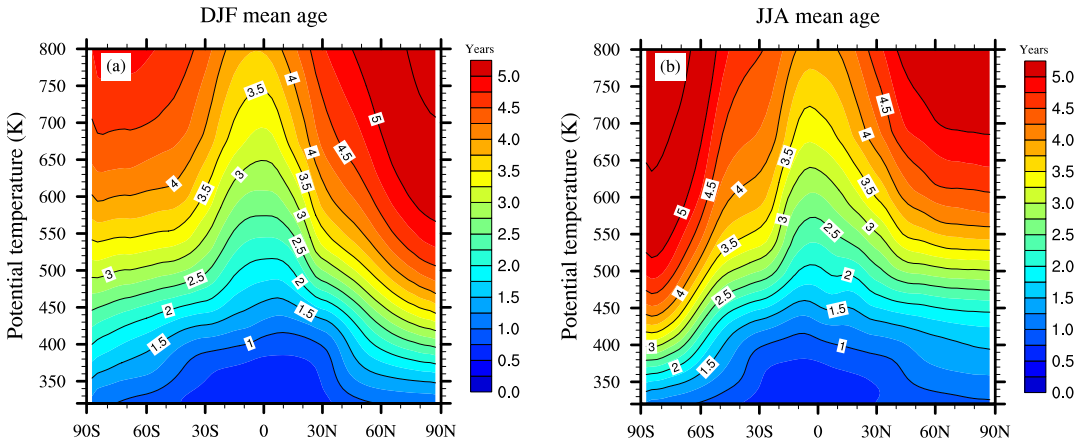

Figure 6.4: Zonal mean distribution of three-year averaged mean age in the Northern Hemisphere winter (DJF) and summer (JJA) obtained by the BIR method. The potential temperature (K) is taken as the vertical coordinate. Figure is taken from Ng21.

6.3 Application to the tropical stratosphere

The profiles of CO_2 and SF_6 ages estimated from eight CUBE/Biak stratospheric air samples are investigated by employing the BIER method in this section. These samples were collected between 17.2 and 28.7 km on 22, 24, 26, and 28 February 2015 (S18). In order to compare properly with the observation, the results estimated from BIER method shown in the rest of this study are interpolated with longitude, latitude and altitude from the nearest neighbors to sampled locations at Biak (1.167° S, 136.1° E). The results are also used to compare to those from Lagrangian backward trajectory method in Ng21. Both the BIER and Lagrangian methods take account of the interannual as well as annual variations of meteorological field, making it possible to compare with the results from CUBE/Biak field campaign, although possible deviations of March 2015 from climatological March cannot be ruled out. Content of this section is mostly reproduced from main results in Ng21.

6.3.1 Mean age from BIER method

The age spectra corresponding to CUBE/Biak cryogenic air samples are shown in Fig. 6.5a for the BIER method. A unimodal distribution (about 0.3 years) and a rapid decrease

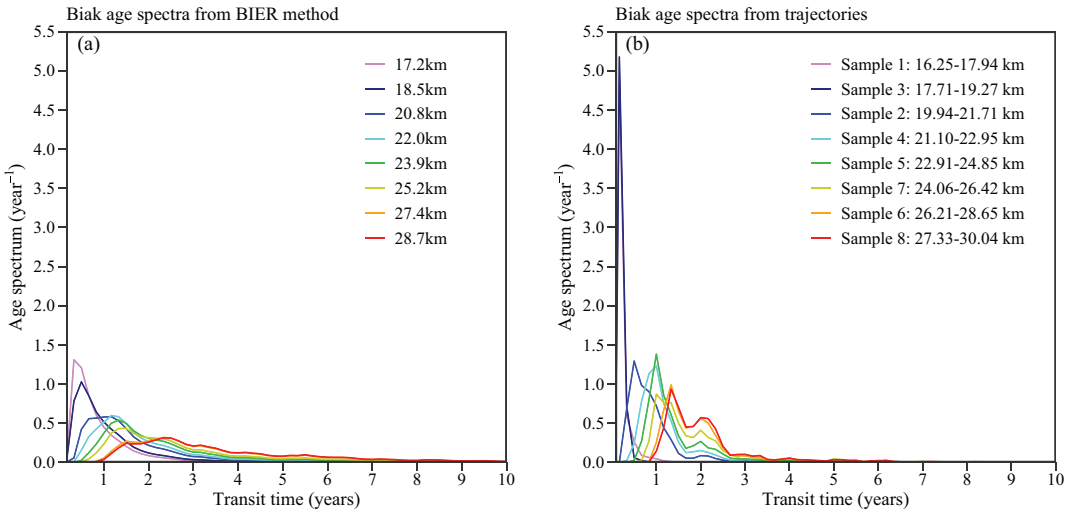

Figure 6.5: Age spectra estimated by the (a) BIER method and (b) Lagrangian method (taken from Ng21) corresponding to the altitudes of eight cryogenic air samples acquired during CUBE/Biak 2015. The temporal resolution is two months in both panels. Figure is taken from Ng21.

(after $\sim$ 1 year) can be observed at some levels above the top of the TTL. Multimodal distributions with a long tail, caused by combination of annual cycle in upwelling and horizontal mixing between the extratropics and tropics, are found above 24 km. As compared to the trajectory age spectra (Fig. 6.5b), we can see that the BIER age spectra show lower peaks with wider band width accompanied by more slowly decaying spectral tail. The long spectral tail considerably affects the magnitude of the mean age (Schoeberl et al., 2005; Li et al., 2012b). The corrected age spectra are used to estimate not only Γ_{corr}, but also the spread of the transit times (Δ) (Hall and Plumb, 1994; Waugh and Hall, 2002). Calculations are extended to other latitudes and heights Figure 6.6 rep-

resents the meridional section of Γ_{corr} in March 2015. The deformation of the contours at 3.0, 3.5, and 4.0 years showing wavy structures in the tropics are due to the downward motion associated with the westerly shear of the QBO. The capability to estimate non-stationary age spectra for complete three-dimensional transport, including mixing, is one of the advantages of the BIER method (Ploeger and Birner, 2016). These values

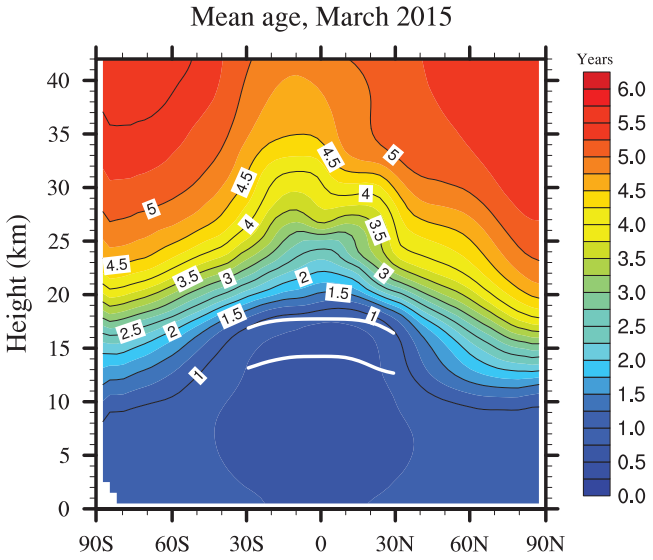

Figure 6.6: Latitude–height section of the mean age in March 2015 estimated by the BIER method using tracers released from January 2005 to March 2015 at the tropical surface (15° S–15° N). The age correction is applied using the transit time from the 4th to 10th years. The 355 K and 400 K isentropes are shown as white lines bounded between 30° N and S indicating the location of Tr_{top} and the top of the TTL, respectively. Figure is taken from Ng21.

of Γ_{corr} are derived by taking Ω at the tropical surface. In contrast, the observational estimates of the mean age by S18 refer to the tracer concentrations in the tropical upper troposphere. Therefore, it is necessary to address the difference in the definition of the reference time from which age counting is started before making direct comparison between the two. As is evident from Chapter 5, the excursion of the tropospheric air to the stratosphere depends on tropospheric transport features, including isentropic mixing with the air in the extratropical LS, and thus the mean age counted from the tropical

surface is not always a sum of the tropospheric residence time and the mean age counted from the TTL. Unfortunately, the BIER calculations assigning Ω to the TTL are confronted with an alternative difficulty due to its large area. In the present analysis, we use the adjusted mean age defined by subtracting the transit time at $\mathrm{Tr_{top}}$ from Γ_{corr} for the comparison with the observational estimates. The mean transit time at the level of $\mathrm{Tr_{top}}$ averaged in the latitude range between 30° N and S is 0.70 ± 0.05 years (mean $\pm$ standard deviation). Then, the adjusted mean age ($\equiv \Gamma_{\mathrm{corr}} - 0.70$ years) is regarded as the stratospheric mean age estimated from the BIER method for the remainder of this paper.

6.3.2 Assessment of mean age profiles

The mean age profiles derived by the BIER method are compared against those estimated by Lagrangian method given by Ng21 and by using observed CO_2 and SF_6 mole fractions given by S18. To avoid confusion, the adjusted mean age estimated by the BIER method ($\Gamma_{\mathrm{corr}} - 0.70$ years) is denoted by Γ_{bir}; the mean age obtained by trajectory calculations (no adjustment after tail correction) is expressed by Γ_{trj}; the observational estimates of the mean age from CO_2 and SF_6 samples are written as Γ_{Cobs} and Γ_{Sobs}, respectively. It is noticed that unlike the correction of tail in the BIER method (Section 6.2), the tail correction applied to the Lagrangian age spectra has little effect on the mean age. Ng21 showed that in the case of Sample 8, for example, Γ_{corr} is found to be 2.16 years, which is only 0.05 years longer than the uncorrected Γ (2.11 years). For the other air samples, the tail correction is smaller than that of Sample 8. Given that the meteorological fields are the same, we could expect that the differences have come from the nature of the trajectory calculations that rely on a finite number of infinitesimal air parcels without taking irreversible mixing into account.

The vertical distributions of mean age are illustrated in Fig. 6.7a, comparing Γ_{bir} (green triangles) and Γ_{trj} (black crosses) with Γ_{Cobs} (blue circles) and Γ_{Sobs} (magenta squares). In general, Γ_{bir} tends to be older than Γ_{trj}, but they are in good agreement below 26 km; Γ_{bir} is only 0.2 years older than Γ_{trj} from 18 km to 26 km. This is quite interesting in view of the different appearance of the age spectra (Fig. 6.5), providing an example wherein varieties of age spectra are possible for a single value of mean age, as is demonstrated in Fig. 3 of Waugh and Hall (2002), because the entire spectral shape cannot be specified solely by the first moment (mean value). In particular, the difference between Γ_{bir} and Γ_{trj} is 0.4 years or less, which roughly corresponds to that of each modal age. It implies that the contribution of the spectral tail is not crucial to mean age in the tropical lowermost stratosphere. Above 26 km, however, Γ_{bir} is $\sim$ 1.2 years older than Γ_{trj}. For these altitudes, the modal ages are found at around 2.4 years in the BIER spectra, whereas the highest peak is maintained to the left-hand-side ($\sim$ 1.4 years) of the bimodal structure in the Lagrangian age spectra. Such a qualitative contrast may have resulted in the large difference in the mean ages. Figure 6.7a shows that Γ_{Cobs} is reasonably well reproduced by Γ_{trj}. That is, both Γ_{Cobs} and Γ_{trj} increase gradually up to 25 km and stay nearly constant above it. In contrast, Γ_{bir} continues to grow up to 29 km, deviating from Γ_{Cobs} at 28 and 29 km. Γ_{Sobs} also increases almost linearly up to 24 km as in Γ_{Cobs}. The reason why Γ_{Cobs} and Γ_{Sobs} appear almost constant over a large area between 25 and 29 km will be understood as follows: under the recognition that the profiles of Γ_{Cobs} and Γ_{Sobs} reflect those of CO_2 and SF_6 concentrations (Fig. 6.8) in the manner wherein the aged (young) air roughly corresponds to low (high) mole fractions. The termination of aging above 25 km is interpreted as the effect of the transport of aged air down to 25 km associated with the secondary circulation of the QBO. The equatorial zonal wind during the sampling period showed a strong westerly shear accompanied by distinct warm anomalies (Fig. 5 of H18), implying a descending motion in the altitudes

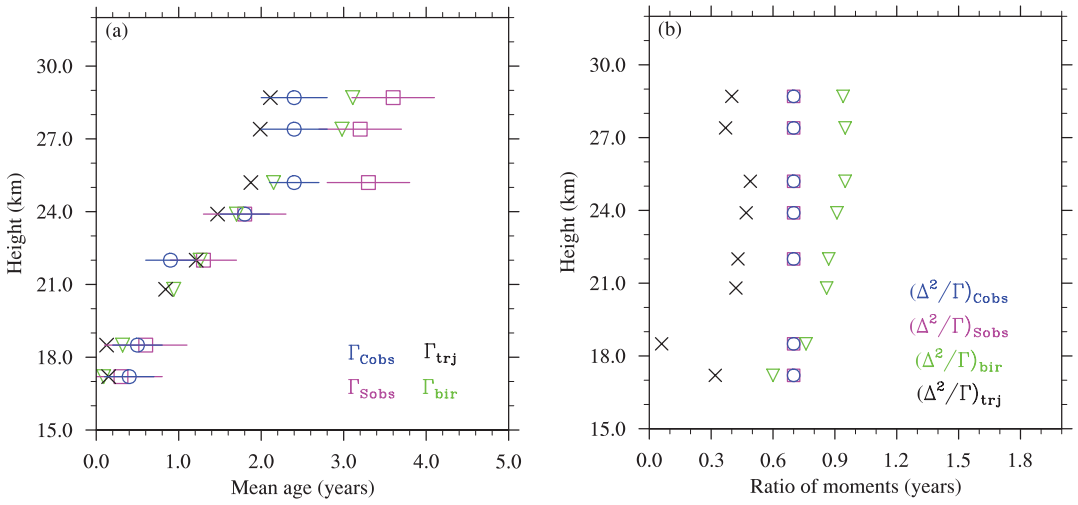

Figure 6.7: Comparison of the vertical profiles of (a) mean age (Γ) and (b) ratio of moments (Δ^2/Γ) estimated by the BIER method (Γ_{bir}; green), back trajectories (Γ_{trj}; black), and cryogenic samples of CO_2 (Γ_{Cobs}; blue) and SF_6 (Γ_{Sobs}; magenta). Γ_{Cobs} and Γ_{Sobs}, taken from S18, are obtained by assuming the ratio of moments Δ^2/Γ to be 0.7 years at all altitudes. Horizontal bars correspond to the uncertainties associated with the laboratory analysis to derive CO_2 and SF_6 concentrations. Figure is taken from Ng21.

between 25 and 28 km. The downward motion was so strong as to make the age spectra at the altitudes of 27 and 29 km almost identical (Fig. 6.5), and displaced the 3.5-year BIER-age contour downward over the equator leading to a wavy structure illustrated on the meridional plane (Fig. 6.6).

6.3.3 Discussion

In the present study, the BIER method has been applied to investigate observationally estimated mean ages in the tropical stratosphere. In some studies, atmospheric transport models are used to conduct clock tracer experiments, in which an inert tracer is released from a region in concentrations linearly increasing with time. In these experiments, the mean age at a location $\boldsymbol{r}$ is directly obtained as the time lag between the occurrences of

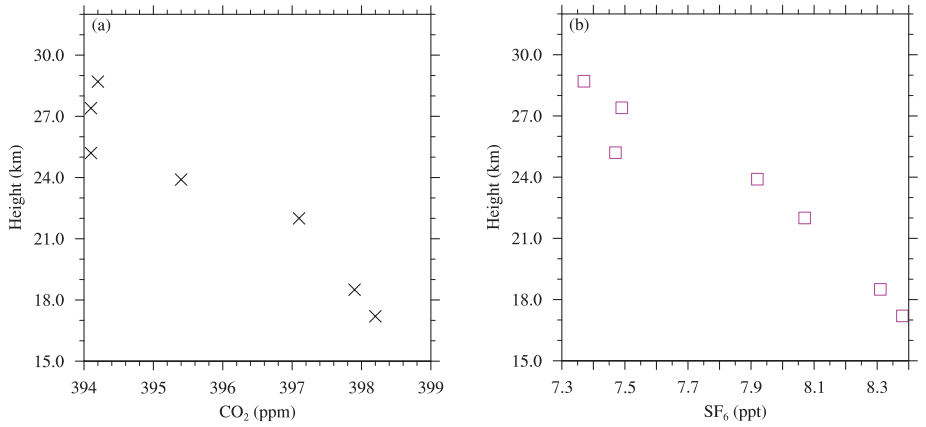

Figure 6.8: Vertical profiles of mole fractions of (a) CO_2 (ppm) and (b) SF_6 (ppt) from air samples (S18).

a particular mixing ratio at $\boldsymbol{r}$ and the source region Ω. Usually, Ω is taken at the ground surface implying that the mean age is defined as the transit time taken all the way from the surface to $\boldsymbol{r}$. However, the problem is that there arise inevitable ambiguities wherein the mean age depends on the setting of Ω through the tropospheric transport properties (e.g., Krol et al., 2018). The situation is the same in the BIER method employed here. As is mentioned in section 6.3.1, we have taken the simplest way wherein Γ_{bir} is adjusted by subtracting the mean transit time at $\mathrm{Tr}_{\mathrm{top}}$ from the estimated mean age to attain correspondence to the observational estimates. Although our transport experiment did not have such an idealized tracer, we have results from a clock-tracer experiment which was conducted with the same experimental conditions as the present study except for the assignment of Ω having been the six lowest layers over the whole globe. Although it is not suitable for making a strict comparison, the estimated mean age (Fig. 6.9) appears slightly younger than that from the BIER method in the troposphere and the extratropical lower stratosphere, probably due to the extended latitudinal coverage of the source region. The mean transit time at the level of $\mathrm{Tr}_{\mathrm{top}}$ between 30° N and S is 0.08 ± 0.05 years, which is much shorter than 0.70 ± 0.05 years in the BIER method

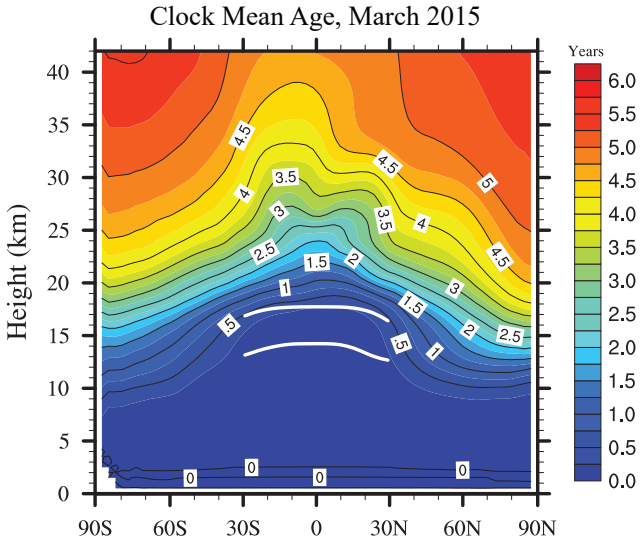

Figure 6.9: Meridional mean age from the model's clock tracer in March 2015 with the source region covering the six lowest layers over the global surface.

(Section 6.3.1). If this difference is taken into account, the mean age of air corresponding to the CUBE/Biak samples agrees reasonably well at all the levels between the two methods.

The assessment of observationally estimated CO_2 and SF_6 mean ages using the BIER method (Section 6.3.2) together with the Lagrangian method given by Ng21 reveals some interesting features. The difference between Γ_{bir} and Γ_{trj} can be understood by the following two factors. One is related to the tail of the age spectrum. It is because the mean age is considerably dependent on the age spectrum tail. In both BIER and Lagrangian methods, the tail is considered as the part of the age spectrum having the transit time longer than 4 years. We found that above 25 km, the contribution of tails to the mean age is about 50–60 % in the BIER method including more than 10 % come from the tail correction (Table 6.1). As discussed in section 6.3.2, the tail correction is not critically important in dealing with the tropical stratosphere with 10-year back trajectories. Due to the strong peaks and short tails of the age spectra, the contribution

of tail to the mean age in Lagrangian method is smaller than 30 %. The tail contribution

Table 6.1: Contributions of the tail and tail correction to the BIER mean age.

Height (km)	17.2	18.5	20.8	22.0	23.9	25.2	27.4	28.7
Tail (%)	14.5	20.7	30.1	34.3	41.1	48.0	58.7	60.1
Tail correction (%)	2.5	4.0	6.1	7.0	8.6	10.4	13.6	14.1

to the BIER mean age in this study is consistent with the calculations from Li et al. (2012b). The contrast between two methods suggests that the entrainment of "ancient" air, incorporated in the BIER method through diffusion and mixing but not considered in the trajectory calculations, makes Γ_{bir} systematically older than Γ_{trj}. The second factor is related to the termination of the trajectory calculations upon arrival at the model top. In the BIER method, the transport calculations extend from the surface to approximately 90 km, while the trajectory calculations are restricted to the region below 1 hPa ($\sim$ 50 km). Ng21 indicated that about 3 % of released parcels (252 out of 8559) in the case of Sample 8 (their Fig. 6a) have reached the top boundary without crossing $\mathrm{Tr}_{\mathrm{top}}$ during the 10-year backward calculation, with the mean transit time of $\sim$ 3.9 years along the back trajectories. These parcels descended from the mesosphere (above 1 hPa) to the high-latitude stratosphere along the deep branch of the BDC, rapidly migrated to the tropics by quasi-isentropic motion, and then reached the tropical middle stratosphere following slow diabatic ascent. It suggests that the mean transit time of such parcels since the last passage through $\mathrm{Tr}_{\mathrm{top}}$ will be at least several years, which is much greater than Γ_{trj} (derived without taking these parcels into account), Γ_{Cobs} and Γ_{Sobs}. Therefore, the omission of these parcels in mean-age estimation must have brought about underestimation in Γ_{trj} relative to Γ_{bir} to some degree even if their relative population is only 3 %. It is also responsible for making Γ_{trj} younger than Γ_{Cobs} and Γ_{Sobs} above 25

km. It means that the absence of mesospheric air parcels in the Lagrangian calculations leads to the younger mean age (Fig. 6.7) as compared with the observational values. The difference between Γ_{trj} and Γ_{Sobs} becomes even larger due to the perceived overestimation of Γ_{Sobs} arising from the mesospheric loss of SF_6 (Andrews et al., 2001a; Reddmann et al., 2001; Waugh and Hall, 2002; Stiller et al., 2012; Ray et al., 2017, S18). That is, the downward transport of SF_6-depleted mesospheric air is misinterpreted in Γ_{Sobs} as the persistence of the aged air that entered the stratosphere when the tropospheric SF_6 mole fraction was low.

For the estimation of Γ_{Cobs}, the constraint on the ratio of moments ($\Delta^2/\Gamma = 0.7$ years; Section 3.3.3) could be crucial in the tropical lower stratosphere where the seasonal variation of the tropospheric CO_2 has not yet decayed appreciably. The ratio of moments was re-examined by Hauck et al. (2019) in their recent study of the method for deriving age spectra. They determined a value of 2.0 years for the annual mean value in the whole lower stratosphere. Our results from the BIER method as well as those from the trajectory method (see Fig. 6.7b) suggest that it is an increasing function of altitude below 25 km, and that the values estimated by the Lagrangian method are significantly smaller than 0.7 years, although those obtained by the BIER method are larger than 0.7 years. A series of Γ_{Cobs} calculations is conducted independently to each level as sensitivity tests by sweeping it covering the range obtained from the BIER and trajectory methods. Fortunately, Γ_{Cobs} stayed within the observational uncertainties when the ratio of moments was changed in the range from 0.05 to 2.00 years (Ng21), and there is no need to revise the former estimates in S18. It was noticed that Γ_{Cobs} becomes a multi-valued function of CO_2 mole fraction at some specific altitude and time due to the propagation of the seasonal cycle of CO_2. Such an occurrence is not unusual in the tropical lower stratosphere, where the tropospheric seasonal cycle is not yet dumped fully. In the case of the CUBE/Biak samples, for example, the CO_2 mole fraction of $\sim$ 397.9 ppm at 18.5

km in February 2015 falls into this singularity, if the ratio of moments is as small as 0.05 years. In such cases, Γ_{Cobs} cannot be uniquely determined from the observed CO_2 mole fraction, emphasizing the importance of the use of realistic values of the ratio of moments in the age estimation from CO_2. The importance of this ratio is also evident from a different perspective, which is the long-term trend of the mean age. The slope of 0.15 ± 0.18 years decade^{-1} (Engel et al., 2017) updated from 0.24 ± 0.22 years decade^{-1} (Engel et al., 2009), in the Northern midlatitude stratosphere is further reduced to 0.07 years decade^{-1} when the the ratio of moments is 1.25 years (Fritsch et al., 2020). In addition to the ratio of moments, the assumption of age spectrum shape as an inverse-Gaussian distribution can also contribute errors to observational mean age estimation above 25 km. That is because this assumed age spectrum represents a smooth shape at all locations, which contradicts the multi-peaks age spectra in both BIER and Lagrangian method above 25 km (Fig.6.5). Thus, the age estimation based on the measurements of trace gases should be made carefully considering the reality of the parameters assumed in the analysis. Current research effort appears to be directed to the development of new methods to estimate age spectrum without assuming its shape. Podglajen and Ploeger (2019) and Hauck et al. (2019, 2020) introduced inverse methods to retrieve age spectrum by taking the advantages of different transit-time dependencies of multiple age tracers. Though the applicabilities of these methods to observed air samples still await further investigation, the future direction will be the application of multiple tracers to better constrain the stratospheric transport features including the mean age.

Chapter 7

Conclusions

In this study, the Boundary Impulse Evolving Response (BIER) method with the aid of an Atmospheric general circulation model-based Chemistry Transport Model (ACTM), nudged to the ERA-Interim temperature and horizontal winds fields, is used to describe the stratospheric transport features through the interpretation of pulse tracer distribution having the TTL and tropical surface source regions. Moreover, the BIER method is applied to assess the mean age profiles estimated from the CO_2 and SF_6 mole fractions observed during the newest CUBE/Biak field campaign over Indonesia. The profile of BIER mean age are also compared with those estimated by the Lagrangian backward trajectory calculations in a three-dimensional wind field of ACTM nudged to ERA-Interim in Ng21. The mean age estimation from observations is dependent upon the long-term aircraft observations as reference and the hypothesized age spectrum as an inverse-Gaussian distribution. In contrast, the BIER method and Lagrangian method have their advantages including straightforwardness in obtaining the age spectrum and independent from measurements. However, unlike the BIER method, the Lagragian method does not factor unresolved mixing and diffusion into the age spectra calculations. The new discoveries

are summarized below.

Concerning the stratospheric transport features, the evolution and distribution of pulse tracers simulated in ACTM show that all transport features, including unresolved diffusive processes, are reasonably well described regardless of the difference of source regions. That is, with both the tropical surface and the TTL, the air is vertically transported by the stratospheric circulation once they enter the tropical lower stratosphere. Then, they are rapidly transported toward high-latitude lowermost stratosphere of both hemispheres due to the eddy mixing around the tropopause and quasi-horizontal transport in the stratosphere. The mixing ratio isopleth patterns tend to be flattened by quasi-horizontal transport and mixing in midlatitudes, especially in winter hemisphere. The tracers released in boreal winter have higher probability to reach high latitudes in comparison with those released in boreal summer.

As for the application of results from the BIER method in assessing the reproducibility of the mean age profiles estimated from the CO_2 and SF_6 mole fractions observed during the CUBE/Biak field campaign, the profiles of CO_2 and SF_6 mean ages are reproduced reasonably well by both BIER and backward trajectory methods, but the agreement is limited to below 25 km. Above 25 km, the SF_6 mean age is generally reproduced well by the BIER method, but is much older than that from Lagrangian estimation. This aging is consistent with the notion that the SF_6 mean age is overestimated due to mixing with SF_6-depleted mesospheric air, whereas the air parcels of mesospheric origin are missing in the Lagrangian age estimation.

This study confirms that the BIER method is capable of capturing all transport features including unresolved diffusive processes which impact the tracer distribution in the stratosphere. The age estimation by this method through assigning the source region to the TTL is not very appropriate due to its wide coverage in latitude and

height. This study also reassures the difficulty in estimating the mean age from tracer observations. The age spectra estimated from our analysis do not support the widely used assumption that the ratio of moments is constant at a value of 0.7 years at all altitudes. Observations of multiple trace gases and other variables independent of mean age, such as the gravitational separation (Ishidoya et al., 2013; Belikov et al., 2019; Sugawara et al., 2018), will be useful to constrain the stratospheric transport features.

Appendix A

Appendix: Spatial variation of tracer mixing ratio

Longitude-latitude distribution of tracer released in January and July at the tropical surface in the troposphere is shown in Figure. A.1 and Figure A.2, respectively. In the first month of simulation, i.e., the month that release is made, the tracer released at the tropical surface source region generally stays inside the latitude band 15° S – 15° N at 1000 hPa (top panel of Figs. A.1 and A.2). At the same time, convective activities transported the tracers upward into the middle troposphere. High concentration is observed in the Western Pacific region in both January and July releases. The meridional transport of tracers is quite slow at 300 hPa. At the first month, concentration of January tracer transported to 100 hPa is more and covers a wider region (bottom panel of Fig. A.1) than July tracer (bottom panel of Fig. A.2). However, the width of zonally distributed tracers in the upper troposphere in both January and July is still narrow. This is consistent with the notion in Chapter 5 concerning the tracer distribution a few months from release.

Figures A.3 and A.4 show the spatial distribution of tracer released at the TTL in January and July 2005, respectively, for the first month of simulation. It is clearly seen that the tracers release in the TTL show relatively fast poleward transport from the source region once pulse tracers were released, suggesting a significant role of the low branches of the BDC in the lower/lowermost stratospheric transport. At the same time, January tracer is transported downward from the poleward edge of the TTL to 300 hPa level along the isentropic intrusion associated with the subtropical jet at around 30° N. By contrast, July tracer is brought down into the troposphere only around Tibet area from the TTL. The strong spread of mixing ratio from the TTL toward the North pole of both tracers and downward the NH troposphere at the subtropical region in winter of January tracer (Fig. A.3) imply that release of tracer at the TTL is somewhat sensitive to quasi-horizontal mixing in the upper troposphere and lower stratosphere region in comparison with the release at the ground.

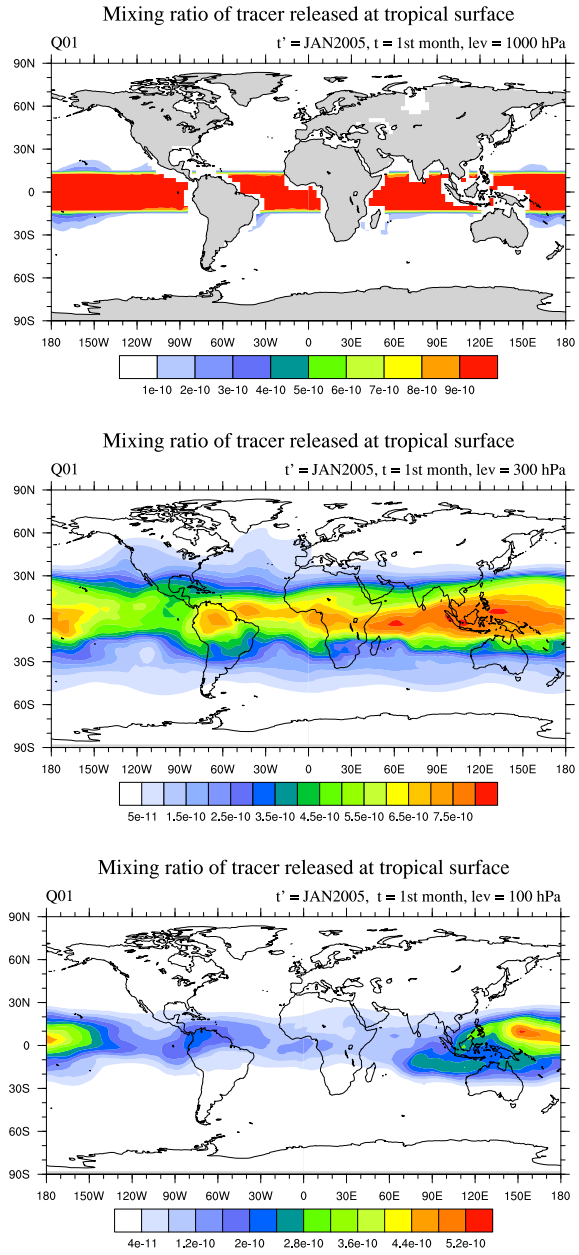

Figure A.1: Longitude-latitude section of mixing ratio of Jan2005-released tracer at the first month of simulation. Top, middle and bottom panels are the distributions at 1000 hPa, 300 hPa and 100 hPa, respectively. The source region is at the tropical surface. t and t' are field time and source time in the BIER method.

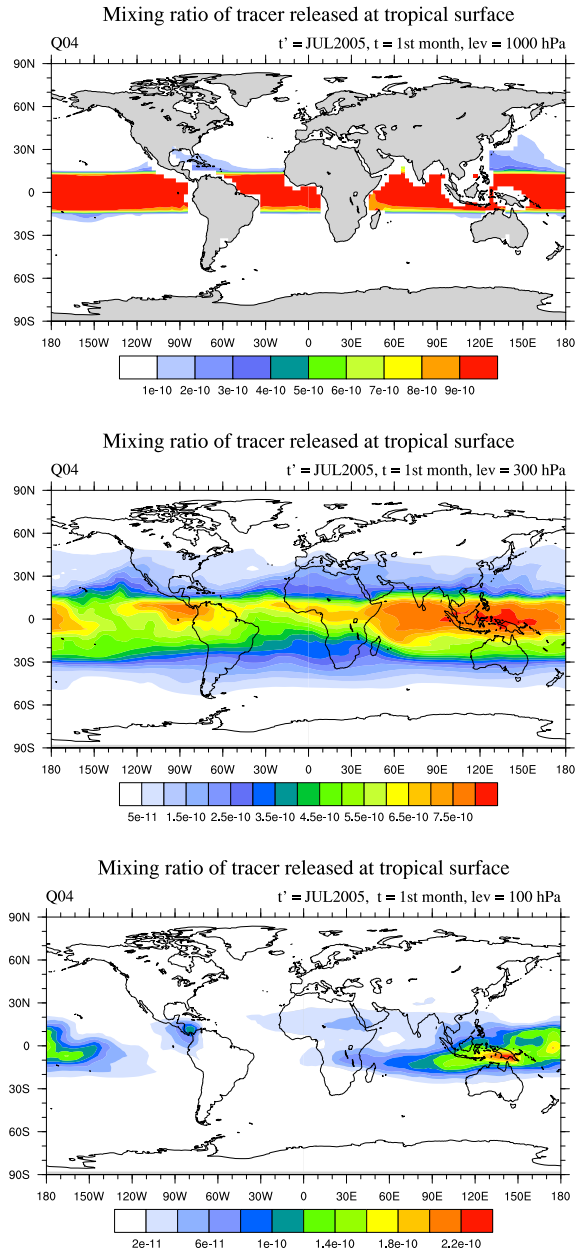

Figure A.2: The same as Fig.A.1 but for tracer released in July 2005.

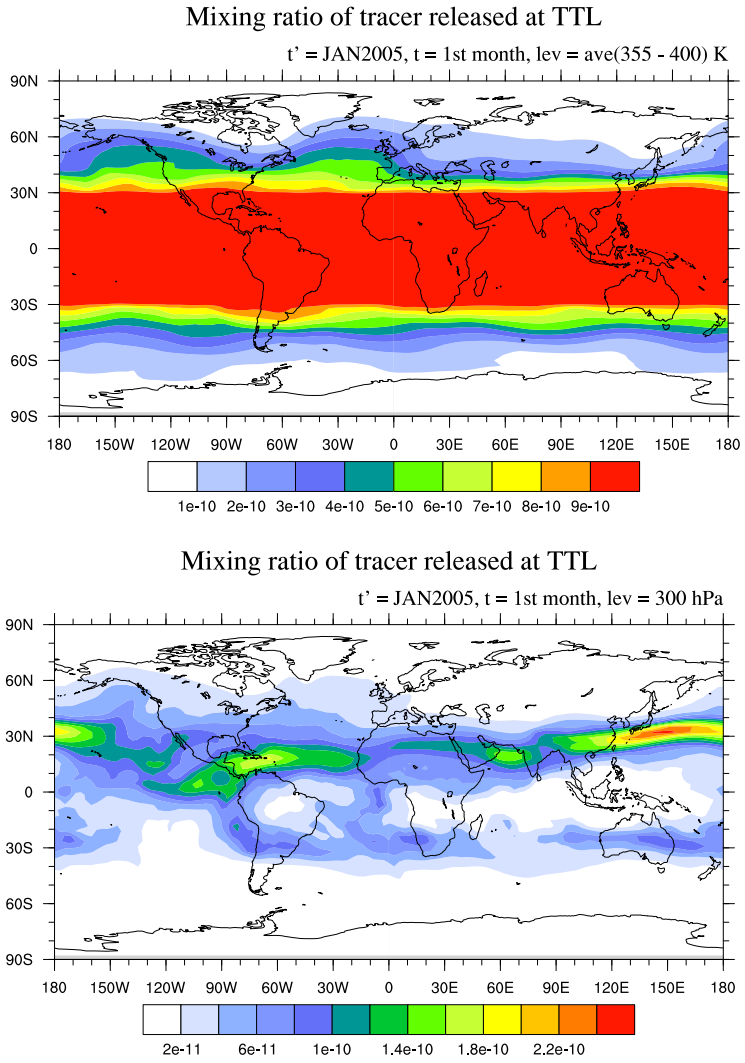

Figure A.3: Longitude-latitude section of mixing ratio of Jan2005-released tracer at the first month of simulation. Top and bottom panels are the distributions at the TTL (averaged from 355 - 400 K), middle troposphere (300 hPa), respectively. The source region is at the tropical tropopause layer.

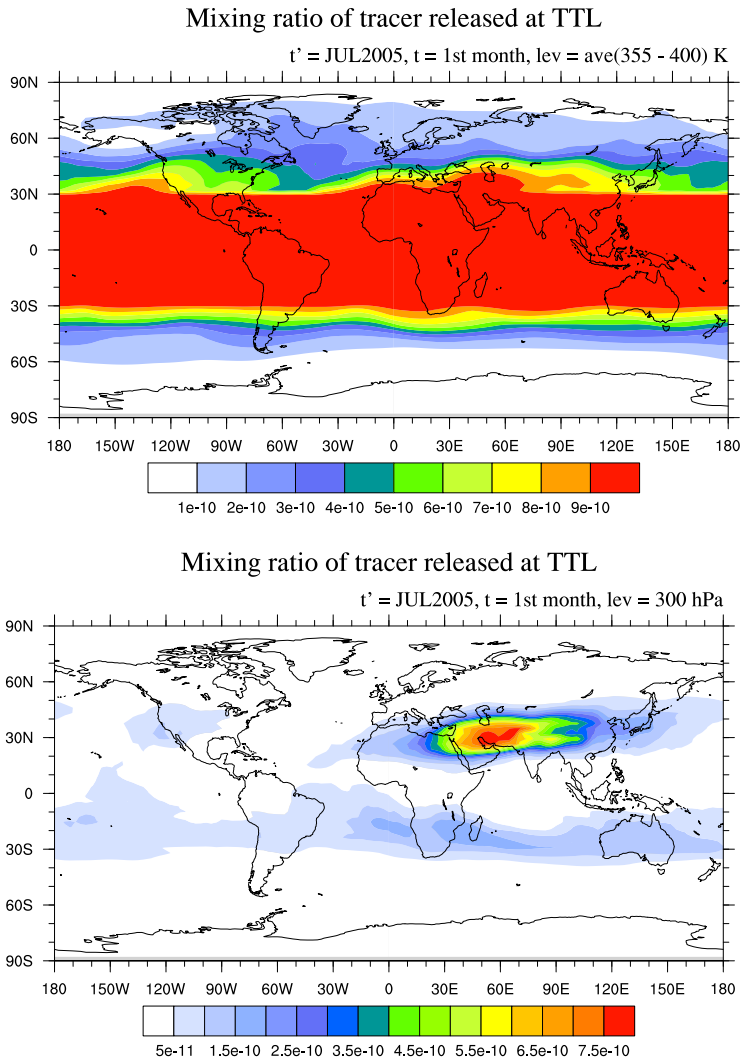

Figure A.4: The same as Fig.A.3 but for tracer released in July 2005.

References

Andrews, D. G., Holton, J. R., and Leovy, C. B.: Middle Atmosphere Dynamics, Academic Press, 1987.

Andrews, A. E., Boering, K. A., Daube, B. C., Wofsy, S. C., Loewenstein, M., Jost, H., Podolske, J. R., Webster, C. R., Herman, R. L., Scott, D. C., Flesch, G. J., Moyer, E. J., Elkins, J. W., Dutton, G. S., Hurst, D. F., Moore, F. L., Ray, E. A., Romashkin, P. A., and Strahan, S. E.: Mean Ages of Stratospheric air Derived from in situ Observations of CO_2, CH_4, and N_2O, J. Geophys. Res., 106, 32 295–32 314, 2001a.

Andrews, A. E., Boering, K. A., Wofsy, S. C., Daube, B. C., Jones, D. B., Alex, S., Loewenstein, M., Podolske, J. R., and Strahan, S. E.: Empirical age spectra for the midlatitude lower stratosphere from in situ observations of CO_2: Quantitative evidence for a subtropical "barrier" to horizontal transport, J. Geophys. Res., 106, 10 257–10 274, 2001b.

Arakawa, A. and Schubert, W. H.:cInteraction of a Cumulus Cloud Ensemble with the Large-Scale Environment, Part I, J. Atmos. Sci., 31, 674–701, 1974.

Austin, J., Wilson, J., Li, F., and Vömel, H.: Evolution of Water Vapor Concentrations and Stratospheric Age of Air in Coupled Chemistry-Climate Model Simulations, J. Atmos. Sci., 64, 905–921, 2007.

Baldwin, M. P., Gray, L. J., Dunkerton, T. J., Hamilton, K., Haynes, P. H., Randel, W. J., Holton, J. R., Alexander, M. J., Hirota, I., Horinouchi, T., Jones, D. B. A., Kinnersley, J. S., Marquardt, C., Sato, K., and Takahashi, M.: The quasi-biennial oscillation, Rev. Geophys., 39, 179–229, 2001.

Belikov, D., Sugawara, S., Ishidoya, S., Hasebe, F., Maksyutov, S., Aoki, S., Morimoto, S., and Nakazawa, T.: Three-dimensional simulation of stratospheric gravitational separation using the NIES global atmospheric tracer transport model, Atmos. Chem. Phys., 19, 5349–5361, https://doi.org/10.5194/acp-19-5349-2019, 2019.

Boering, K. A., Wofsy, S. C., Daube, B. C., Schneider, H. R., Loewenstein, M., Podolske, J. R., and Conway, T. J.: Stratospheric Mean Ages and Transport Rates from Observations of Carbon Dioxide and Nitrous Oxide, Science, 274, 1340–1343, 1996.

Brewer, A. W.: Evidence for a world circulation provided by the measurements of helium and water vapour distribution in the stratosphere, Quart. J. Roy. Meteorol. Soc., 75, 351–363, 1949.

Butchart, N., Cionni, I., Eyring, V., Shepherd, T. G., Waugh, D. W., Akiyoshi, H., Austin, J., Brühl, C., Chipperfield, M. P., Cordero, E., Dameris, M., Deckert, R., Dhomse, S., Frith, S. M., Garcia, R. R., Gettelman, A., Giorgetta, M. A., Kinnison, D. E., Li, F., Mancini, E., McLandress, C., Pawson, S., Pitari, G., Plummer, D. A., Rozanov, E., Sassi, F., Scinocca, J. F., Shibata, K., Steil, B., and Tian, W.: Chemistry-Climate Model Simulations of Twenty-First Century Stratospheric Climate and Circulation Changes, J. Climate, 23, 5349–5374, doi:10.1175/2010JCLI3404.1, 2010.

Butchart, N.: The Brewer-Dobson Circulation, Rev. Geophys., 52, 157–184, doi:10.1002/2013RG000448, 2014.

Charney, J. G.,and Drazin, P. G.: Propagation of Planetary-scale disturbances from the lower into the upper atmosphere, J. Geophys. Res., 66, 1, 1961.

Chen, P.: Isentropic cross-tropopause mass exchange in the extratropics, J. Geophys. Res., 100, 16,661–16,673, doi:10.1029/95JD01264, 1995.

Chen, B., Xu, X. D., Yang, S., and Zhao, T. L.: Climatological perspectives of air transport from atmospheric boundary layer to tropopause layer over Asian monsoon regions during boreal summer inferred from Lagrangian approach, Atmos. Chem. Phys. Discuss., 12, 4185–4219, doi:10.5194/acpd-124185-2012, 2012.

Chrysanthou, A., Maycock, A. C., Chipperfield, M. P., Dhomse, S., Garny, H., Kinnison, D., Akiyoshi, H., Deushi, M., Garcia, R. R., Jöckel, P., Kirner, O., Pitari, G., Plummer, D. A., Revell, L., Rozanov, E., Stenke, A., Tanaka, T. Y., Visioni, D., and Yamashita, Y.: The effect of atmospheric nudging on the stratospheric residual circulation in chemistry–climate models, Atmos. Chem. Phys., 19, 11 559–11 586 https://doi.org/10.5194/acp-19-11559-2019, 2019.

Colella, P., and Woodward P. R.: The Piecewise Parabolic Method (PPM) for Gas-Dynamic Simulations, J. Comput. Phys., 54, 174–201, 1984.

Dee, D. P., Uppala, S. M., Simmons, A. J., Berrisford, P., Poli, P., Kobayashi, S., Andrae, U., Balmaseda, M. A., Balsamo, G., Bauer, P., Bechtold, P., Beljaars, A. C. M., van de Berg, L., Bidlot, J., Bormann, N., Delsol, C., Dragani, R., Fuentes, M., Geer, A. J., Haimberger, L., Healy, S. B., Hersbach, H., Hólm, E. V., Isaksen, L., Kållberg, P., Köhler, M., Matricardi, M., McNally, A. P., Monge-Sanz, B. M., Morcrette, J. J., Park, B. K., Peubey, C., de Rosnay, P., Tavolato, C., Thépaut, J. N., and Vitart, F.: The ERA-Interim Reanalysis: Configuration and Performance of the Data Assimilation System, Quart. J. Roy. Meteorol. Soc., 137, 553–597, 2011.

Diallo, M., Legras, B., and Chédin, A.: Age of Stratospheric air in the ERA-Interim, Atmos. Chem. Phys., 12, 12 133–12 154, doi:10.5194/acp-12-12133-2012, 2012.

Dobson, G. M. B.: Origin and distribution of the polyatomic molecules in the atmosphere, Proc. Roy. Soc. London, A236, 187–193, 1956.

Dragani, R.: On the quality of the ERA-Interim ozone reanalyses: comparisons with satellite data, Q. J. Roy. Meteor. Soc., 137, 1312–1326, https://doi.org/10.1002/qj.821, 2011.

Dunkerton, T. J.: On the mean meridional mass motions of the stratosphere and mesosphere, J., Atmos. Sci., 35, 2325–2333, 1978.

Ehhalt D. H., Rohrer, F., Schauffler, S., and Prather, M.: On the decay of stratospheric pollutants: Diagnosing the longest-lived eigenmode, J. Geophys. Res., 109, 347–350, doi:10.1029/2003JD004029, 2004.

Elkins, J. W., Fahey, D. W., Gilligan, J. M., Dutton, G. S., Baring, T. J., Volk, C. M., Dunn, R. E., Myers, R. C., Montzka, S. A., Wamsley, P. R., Hayden, A. H., Butler, J. H., Thompson, T. M., Swanson, T. H., Dlugokencky, E. J., Novelli, P. C., Hurst, D. F., Lobert, J. M., Ciciora, S. J., McLaughlin, R. J., Thompson, T. L., Winkler, R. H., Fraser, P. J., Steele, L. P., and Lucarelli, M. P.: Airborne gas chromatograph for in situ measurements of long-lived species in the upper troposphere and lower stratosphere, Geophys. Res. Lett., 23, 347–350, 1996.

Engel, A., Strunk, M., Müller, M., Haase, H.-P., Poss, C., Levin, I., and Schmidt, U.: Temporal Development of Total Chlorine in the High-Latitude Stratosphere Based on Reference Distributions of Mean age Derived from CO_2 and SF_6, J. Geophys. Res., 107, 4136, doi:10.1029/2001JD000584, 2002.

Engel, A., Möbius, T., Bönisch, H., Schmidt, U., Heinz, R., Levin, I., Atlas, E., Aoki, S., Nakazawa, T., Sugawara, S., Moore, F., Hurst, D., Elkins, J., Schauffler, S., Andrews, A., and Boering, K.: Age of Stratospheric air Unchanged within Uncertainties Over the Past 30 Years, Nature Geosci., 2, 28–31, 2009.

Engel, A., Bönisch, H., Ullrich, M., Sitals, R., Membrive, O., Danis, F., and Crevoisier, C.: Mean age of stratospheric air derived from AirCore observations, Atmos. Chem. Phys., 17, 6825–6838, https://doi.org/10.5194/acp-17-6825-2017, 2017.

Fritsch, F., Garny, H., Engel, A., Bönisch, H., and Eichinger, R.: Sensitivity of Age of Air Trends on the derivation method for non-linear increasing inert SF_6, Atmos. Chem. Phys., 20, 8709–8725, https://doi.org/10.5194/acp-20-8709-2020, 2020.

Fueglistaler, S., Bonazzola, M., Haynes, P. H., and Peter, T.: Stratospheric water vapor predicted from the Lagrangian temperature history of air entering the stratosphere in the tropics, J. Geophys. Res., 110, D08107, doi:10.1029/2004JD005516, 2005.

Fueglistaler, S., Dessler, A., Dunkerton, T., Folkins, I., Fu, Q., and Mote, P.: Tropical tropopause layer, Rev. Geophys., 47, RG1004, doi:10.1029/2008RG000267, 2009.

Fujiwara, M., Vömel, H., Hasebe, F., Shiotani, M., Ogino, S. Y., Iwasaki, S., Nishi, N., Shibata, T., Shimizu, K., Nishimoto, E., Valverde-Canossa, J. M., Selkirk, H. B., and Oltmans, S. J.: Seasonal to decadal variations of water vapor in the tropical lower stratosphere observed with balloon-borne cryogenic frostpoint hygrometers, J. Geophys. Res., 115, D18304, doi: 10.1029/2010JD014179, 2010.

Garcia, R. R., Randel, W. J., and Kinnison, D. E.: On the Determination of Age of Air Trends from Atmospheric Trace Species, J. Atmos. Sci., 68, 139–154, DOI:10.1175/2010JAS3527.1, 2011.

Haine, T. W. N., Zhang, H., Waugh, D. W., and Holzer, M.: On Transit-Time Distributions in Unsteady Circulation Models, Ocean Modell., 21, 35–45, doi:10.1016/j.ocemod.2007.11.004, 2008.

Hall, T. M. and Plumb, R. A.: Age as a Diagnostic of Stratospheric Transport, J. Geophys. Res., 99, 1059–1070, 1994.

Hall, T. M., Waugh, D. W., Boering, K. A., and Plumb, R. A.: Evaluation of Transport in Stratospheric Models, J. Geophys. Res., 104, 18 815–18 839, 1999.

Harnisch, J., Borchers, R., Fabian, P., and Maiss, M.: Tropospheric trends for CF_4 and C_2F_6 since 1982 derived from SF_6 dated stratospheric air, Geophys. Res. Lett., 23, 1099–1102, 1996.

Hasebe, F., and Noguchi, T.: A Lagrangian description on the troposphere-to-stratosphere transport changes associated with the stratospheric water drop around the year 2000, Atmos. Chem. Phys., 16, 4235–4249, https://doi.org/10.5194/acp-16-4235-2016, 2016.

Hasebe, F., Aoki, S., Morimoto, S., Inai, Y., Nakazawa, T., Sugawara, S., Ikeda, C., Honda, H., Yamazaki, H., Halimurrahman, Komala, N., Putri, F., Budiyono, A., Soedjarwo, M., Ishidoya, S., Toyoda, S., Shibata, T., Hayashi, M., Eguchi, N., Nishi, N., Fujiwara, M., Ogino, S., Shiotani, M., and Sugidachi, T.: Coordinated Upper-Troposphere-to-Stratosphere Balloon Experiment in Biak (CUBE/Biak), Bull. Amer. Meteor. Soc., 99, 1213–1230, doi:10.1175/BAMS-D-16-0289.1, 2018.

Hauck, M., Fritsch, F., Garny, H., and Engel, A.: Deriving stratospheric age of air spectra using an idealized set of chemically active trace gases, Atmos. Chem. Phys., 19, 5269–5291, https://doi.org/10.5194/acp-19-5269-2019, 2019.

Hauck, M., Bönisch, H., Hoor, P., Keber, T., Ploeger, F., Schuck, T. J., and Engel, A.: A convolution of observational and model data to estimate age of air spectra in the northern hemispheric lower stratosphere, Atmos. Chem. Phys., 20, 8763–8785, doi:10.5194/acp-20-8763-2020, 2020.

Holton, J. R.: An Introduction to Dynamic Meteorology, Fourth Edition, Elsevier Academic Press, 2004.

Holzer, M., McKendry, J. G., and Jaffe, D. A.: Springtime trans-Pacific atmospheric transport from east Asia: A transit-time probability density function approach, J. Geophys. Res., 108, D22, 4708, doi:10.1029/2003JD003558, 2003.

Ishidoya, S., Sugawara, S., Morimoto, S., Aoki, S., Nakazawa, T., Honda, H., and Murayama, S.: Gravitational separation in the stratosphere – a new indicator of atmospheric circulation, Atmos. Chem. Phys., 13, 8787–8796, doi:10.5194/acp-13-8787-2013, 2013.

Ishijima, K., Patra, P. K., Takigawa, M., Machida, T., Matsueda, H., Sawa, Y., Steele, L. P., Krummel, P. B., Langenfelds, R. L., Aoki, S., and Nakazawa, T.: Stratospheric Influence on the Seasonal Cycle of Nitrous Oxide in the Troposphere as Deduced from Aircraft Observations and Model Simulations, J. Geophys. Res., 115, D20308, doi:10.1029/2009JD013322, 2010.

Jones, R. L., and Pyle, J. A.: Observations of CH_4 and N_2O by the NIMBUS 7 SAMS: A comparison with in situ data and two-dimensional numerical model calculations, J. Geophys. Res., 89, D4, 5263–5279, 1984.

Kida, H.: General Circulation of Air Parcels and Transport Characteristics Derived from a Hemispheric GCM Part 2. Very Long-Term Motions of Air Parcels in the Troposphere and Stratosphere, J. Meteorol. Soc. Japan, 61, 510–523, 1983.

Kinoshita, T., Sato, K., Ishijima, K., Takigawa, M., and Yamashita, Y.: Formulation of three-dimentional quasi-residual mean flow balanced with diabatic heating rate and potential vorticity flux, J. Atmos. Sci., 76, 851–863, https://doi.org/10.1175/JAS-D-18-0085.1.

Krol, M., de Bruine, M., Killaars, L., Ouwersloot, H., Pozzer, A., Yin, Y., Chevallier, F., Bousquet, P., Patra, P., Belikov, D., Maksyutov, S., Dhomse, S., Feng, W., and Chipperfield, M. P.: Age of Air as a Diagnostic for Transport Timescales in Global Models, Geosci. Model Dev., 11, 3109–3130, https://doi.org/10.5194/gmd-11-3109-2018, 2018.

Li, D., and Shine, K. P.: UK Universities Global Atmospheric Modelling Programme (UGAMP) Global Ozone Climatology Project Dataset, NCAS British Atmospheric Data Centre, http://catalogue.ceda.ac.uk/uuid/bff84b935ce5aa9f04624777b0eea507, 1999.

Li, F., Waugh, D. W., Douglass, A. R., Newman, P. A., Pawson, S., Stolarski, R. S., Strahan, S. E., and Nielsen, J. E.: Seasonal Variations of Stratospheric age Spectra in the Goddard Earth Observing System Chemistry Climate Model (GEOSCCM), J. Geophys. Res., 117, D05134, doi:10.1029/2011JD016877, 2012a.

Li, F., Waugh, D. W., Douglass, A. R., Newman, P. A., Strahan, S. E., Ma, J., Nielsen, J. E., and Liang, Q.: Long-Term Changes in Stratospheric age Spectra in the 21st Century in the Goddard Earth Observing System Chemistry-Climate Model (GEOSCCM), J. Geophys. Res., 117, D20119, doi:10.1029/2012JD017905, 2012b.

Lin, S.-J. and Rood, R. B.: Multidimensional Flux-Form Semi-Lagrangian Transport Schemes, Mon. Wea. Rev., 124, 2046–2070, 1996.

Machida, T., Matsueda, H., Sawa, Y., Nakagawa, Y., Hirotani, K., Kondo, N., Goto, K.,

Nakazawa, N., Ishikawa, K., and Ogawa, T.: Worldwide measurements of atmospheric CO_2 and other trace gas species using commercial airlines, J. Atmos. Ocean. Tech., 25, 1744–1754, https://doi.org/10.1175/2008JTECHA1082.1, 2008.

Matsueda, H., Machida, T., Sawa, Y., and Niwa, Y.: Long- term change of CO_2 latitudinal distribution in the upper troposphere, Geophys. Res. Lett., 42, 2508–2514, https://doi.org/10.1002/2014GL062768, 2015.

McFarlane, N. A.: The effect of orographically excited gravity wave drag on the general circulation of the lower stratosphere and troposphere, J. Atmos. Sci., 44, 1775–1800, 1987.

McIntyre, M. E., and Palmer, T. N.: The 'surf zone' in the stratosphere, J. Atmos. Terr. Phys, 9, 825–849, 1984.

Mellor, G. L. and Yamada, T.: Development of a Turbulence Closure Model for Geophysical Fluid Problems, Rev. Geophys. Space Phys., 20, 851–875, 1982.

Molina, M. J. and Rowland, F. S.: Stratospheric sink for chlorofluoromethanes: Chlorine atom-catalysed destruction of ozone, Nature, 249, 810–812, 1974.

Mote, P. W., Rosenlof, K. H., McIntyre, M. E., Carr, E. S., Gille, J. C., Holton, J. R., Kinnersley, J. S., Pumphrey, H. C., Russell III, J. M., and Waters, J. W.: An atmospheric tape recorder: The imprint of tropical tropopause temperatures on stratospheric water vapor, J. Geophys. Res., 101, 3989–4006, 1996.

Nakazawa, T., Machida, T., Sugawara, S., Murayama, S., Morimoto, S., Hashida, G., Honda, H., and Itoh, T.: Measurements of the Stratospheric Carbon Dioxide Concentration Over Japan Using a Balloon-Borne Cryogenic Sampler, Geophys. Res. Lett., 22, 1229–1232, 1995.

Neu, J. L. and Plumb, R. A.: Age of air in a "Leaky Pipe" Model of Stratospheric Transport, J. Geophys. Res., 104, 19 243–19 255, 1999.

Nguyen, T. H., Ishijima, K., Sugawara, S., Hasebe, F.: Application of a nudged GCM to the interpretation of the mean age of air derived from stratospheric samples in the tropics, J. Meteorol. Soc. Japan, 99, doi:10.2151/jmsj.2021-056, 2021.

Numaguti, A., Takahashi, M., Nakajima, T., and Sumi, A.: Development of CCSR/NIES Atmospheric General Circulation Model, CGER's Supercomput. Monogr. Rep. 3, pp. 1–48, Natl. Inst. for Environ. Stud., Tsukuba, Japan, 1997.

Onogi, K., Tsutsui, J., Koide, H., Sakamoto, M., Kobayashi, S., Hatsushika, H., Matsumoto, T., Yamazaki, N., Kamahori, H., Takahashi, K., Kadokura, S., Wada, K., Kato, K., Oyama, R., Ose, T., Mannoji, N., and Taira, R.: The JRA-25 reanalysis, J. Meteorol. Soc. Japan, 85(3), 369–432, 2007.

Park, S., Jiménez, R., Daube, B. C., Pfister, L., Conway, T. J., Gottlieb, E. W., Chow, V. Y., Curran, D. J., Matross, D. M., Bright, A., Atlas, E. L., Bui, T. P., Gao, R.-S., Twohy, C. H., and Wofsy, S. C.: The CO2 tracer clock for the Tropical Tropopause Layer, Atmos. Chem. Phys., 7, 3989–4000, doi:10.5194/acp-7-39892007, 2007.

Patra, P. K., Lal, S., Subbaraya, B. H., Jackman, C. H., and Rajaratnam, P.: Observed Vertical Profile of Sulphur Hexafluoride (SF_6) and its Atmospheric Applications, J. Geophys. Res., 102, 8855–8859, 1997.

Patra, P. K., Takigawa, M., Dutton, G. S., Uhse, K., Ishijima, K., Lintner, B. R., Miyazaki, K., and Elkins, J. W.: Transport mechanisms for synoptic, seasonal and interannual SF_6 variations and "age" of air in troposphere, Atmos. Chem. Phys., 9, 1209–1225, doi:10.5194/acp-9-1209-2009, 2009.

Patra, P. K., Takigawa, M., Watanabe, S., Chandra, N., Ishijima, K., and Yamashita, Y.: Improved Chemical Tracer Simulation by MIROC4.0-based Atmospheric Chemistry-Transport Model (MIROC4-ACTM), SOLA, 14, 91-96, 2018.

Ploeger, F. and Birner, T.: Seasonal, Inter-Annual Variability of Lower Stratospheric age of air Spectra, Atmos. Chem. Phys., 16, 10 195–10 213, doi:10.5194/acp-16-10195-2016, 2016.

Plumb, R. A.: A "Tropical Pipe" Model of Stratospheric Transport, J. Geophys. Res., 101, 3957–3972, 1996.

Plumb, R. A., and Eluszkiewicz, J.: The Brewer-Dobson circulation: Dynamics of the tropical upwelling, J. Atmos. Sci., 56, 868–890, 1999.

Plumb, R. A.: Stratospheric transport. J. Meteor. Soc. Japan, 80, 793–809, 2002.

Plumb, R. A.: Tracer interrelationships in the stratosphere, Rev. Geophys., 45, RG4005, doi:10.1029/2005RG000179, 2007.

Plumb, R. A. and Bell, R. C.: A model of the quasi-biennial oscillation on an equatorial beta-plane, Quart. J. Roy. Meteorol. Soc., 108, 335–352, 1982.

Podglajen, A., and Ploeger, F.: Retrieving the age of air spectrum from tracers: principle and method, Atmos. Chem. Phys., 19, 1767–1783, doi:10.5194/acp-19-1767-2019, 2019.

Randel, W. J., Gille, J. C., Roche, A. E., Kumer, J. B., Mergenthaler, J. L., Waters, J. W., Fishbein, E. F., and Lahoz, W. A.: Stratospheric transport from the tropics to middle latitudes by planetary-wave mixing, Nature, 365, 533–535, 1993.

Randel, W. J., Wu, F., Vömel, H., Nedoluha, G. E., and Forster, P.: Decreases in stratospheric water vapor after 2001: Links to changes in the tropi-

cal tropopause and the Brewer-Dobson circulation, J. Geophys. Res., 111, D12312, doi:10.1029/2005JD006744, 2006.

Ray, E. A., Moore, F. L., Elkins, J. W., Dutton, G. S., Fahey, D. W., Vömel, H., Oltmans, S. J., and Rosenlof, K. H.: Transport into the Northern Hemisphere lowermost stratosphere revealed by in situ tracer measure- ments, J. Geophys. Res., 104, D21, 26,565–26,580, 1999.

Ray, E. A., Moore, F. L., Rosenlof, K. H., Davis, S. M., Sweeney, C., Tans, P., Wang, T., Elkins, J. W., Bönisch, H., Engel, A., Sugawara, S., Nakazawa, T., and Aoki, S.: Improving stratospheric transport trend analysis based on SF6 and CO2 measurements, J. Geophys. Res., 119, 14, 110–14,128, https://doi.org/10.1002/2014JD021802, 2014.

Ray, E. A., Moore, F. L., Elkins, J. W., Rosenlof, K. H., Laube, J. C., Röckmann, T., Marsh, D. R., and Andrews, A. E.: Quantification of the SF_6 Lifetime Based on Mesospheric Loss Measured in the Stratospheric Polar Vortex, J. Geophys. Res. Atmos., 122, 4626–4638, doi:10.1002/2016JD026198, 2017.

Reddmann, T., Ruhnke, R., and Kouker, W.: Three-dimensional model simulations of SF_6 with mesospheric chemistry, J. Geophys. Res., 106, D13, doi:10.1029/2000JD900700, 2001.

Reithmeier, C., Sausen, R., and Grewe, V.: Investigating Lower Stratospheric Model Transport: Lagrangian Calculations of Mean age and age Spectra in the GCM ECHAM4, Clim. Dyn., 30, 225–238, doi:10.1007/s00382-007-0294-1, 2008.

Riese, M., Ploeger, F., Rap, A., Vogel, B., Konopka, P., Dameris, M., and Forster, P.: Impact of uncertainties in atmospheric mixing on simulated UTLS composition and related radiative effects, J. Geophys. Res., 117, D16305, doi:10.1029/2012JD017751, 2012.

Rosenlof, K. H., Tuck, A. F., Kelly, K. K., Russell III, J. M., and McCormick, M. P.: Hemispheric asymmetries in water vapor and inferences about transport in the lower stratosphere, J. Geophys. Res., 102, 13,213–13,234, doi:10.1029/97JD00873, 1997.

Sawa, Y., Machida, T., and Matsueda, H.: Seasonal variations of CO_2 near the tropopause observation by commercial aircraft, J. Geophys. Res., 113, D23301, https://doi.org/10.1029/2008JD010568, 2008.

Scheele, M. P., Siegmund, P. C., and Velthoven, P. F. J.: Stratospheric age of air computed with trajectories based on various 3D-Var and 4D-Var data sets, Atmos. Chem. Phys., 5, 1–7, 1680-7324/acp/2005-5-1, 2005.

Schmidt, U., Kulessa, G., Klein, E., Röth, E. P., Fabian, P., and Borchers, R.: Intercomparison of balloon-borne cryogenic whole air samplers during the MAP/GLOBUS 1983 campaign, Planet. Space Sci., 35(5), 647–656, 1987.

Schmidt, U., and Khedim, A.: In situ measurements of carbon dioxide in the winter Arctic vortex and at midlatitudes: An indicator of the 'age' of stratospheric air, Geophys. Res. Lett., 18, 4, 763–766, 1991.

Schoeberl, M. R., Douglass, A. R., Zhu, Z., and Pawson, S.: A comparison of the lower stratospheric age spectra derived from a general circulation model and two data assimilation systems, J. Geophys. Res., 108(D3), 4113, doi:10.1029/2002JD002652, 2003.

Schoeberl, M. R., Douglass, A. R., Polansky, B., Boone, C., Walker, K. A., and Bernath, P.: Estimation of Stratospheric age Spectrum from Chemical Tracers, J. Geophys. Res., 110, D21303, doi:10.1029/2005JD006125, 2005.

Solomon, S., Rosenlof, K. H., Portmann, R. W., Daniel, J. S., Davis, S. M., Sanford,

T. J., and Plattner, G.-K.: Contributions of Stratospheric Water Vapor to Decadal Changes in the Rate of Global Warming, Science, 327, 1219–1223, 2010.

Stiller, G. P., von Clarmann, T., Haenel, F., Funke, B., Glatthor, N., Grabowski, U., Kellmann, S., Kiefer, M., Linden, A., Lossow, S., and López-Puertas, M.: Observed Temporal Evolution of Global Mean age of Stratospheric air for the 2002 to 2010 Period, Atmos. Chem. Phys., 12, 3311–3331, doi:10.5194/acp-12-3311-2012, 2012.

Strahan, S. E., Douglass, A. R., Nielsen, J. E., Boering, K. A.: The CO_2 seasonal cycle as a tracer of transport, J. Geophys. Res., 103, D12, 13,729–13,741, 1998.

Sugawara, S., Ishidoya, S., Aoki, S., Morimoto, S., Nakazawa, T., Toyoda, S., Inai, Y., Hasebe, F., Ikeda, C., Honda, H., Goto, D., and Putri, F. A.: Age and Gravitational Separation of the Stratospheric air Over Indonesia, Atmos. Chem. Phys., 18, 1819–1833, https://doi.org/10.5194/acp-18-1819-2018, 2018.

Yulaeva, E., Holton, J. R., and Wallace, J. M.: On the Cause of the Annual Cycle in Tropical Lower-Stratospheric Temperatures, J. Atmos. Sci., 51, 169–174, 1994.

Waugh, D. W. and Hall, T. M.: Age of stratospheric air: Theory, observations, and models, Rev. Geophys., 40, 1010, doi:10.1029/2000RG000101, 2002.

World Meteorological Organization, Scientific Assessment of Ozone Depletion: 1994, Rep. 37, Geneva, 1995.

World Meteorological Organization, Scientific Assessment of Ozone Depletion: 2006, Global Ozone Research and Monitoring Project–Report No. 50, 572 pp., Geneva, Switzerland, 2007.

Scherer, M., Vömel, H., Fueglistaler, S., Oltmans, S. J., and Staehelin, J.: Trends and variability of midlatitude stratospheric water vapour deduced from the re-evaluated Boulder balloon series and HALOE, Atmos. Chem. Phys., 8, 1391–1402, 2008.

Waugh, D.: The age of stratospheric air, Nature Geoscience, 2, 2009.